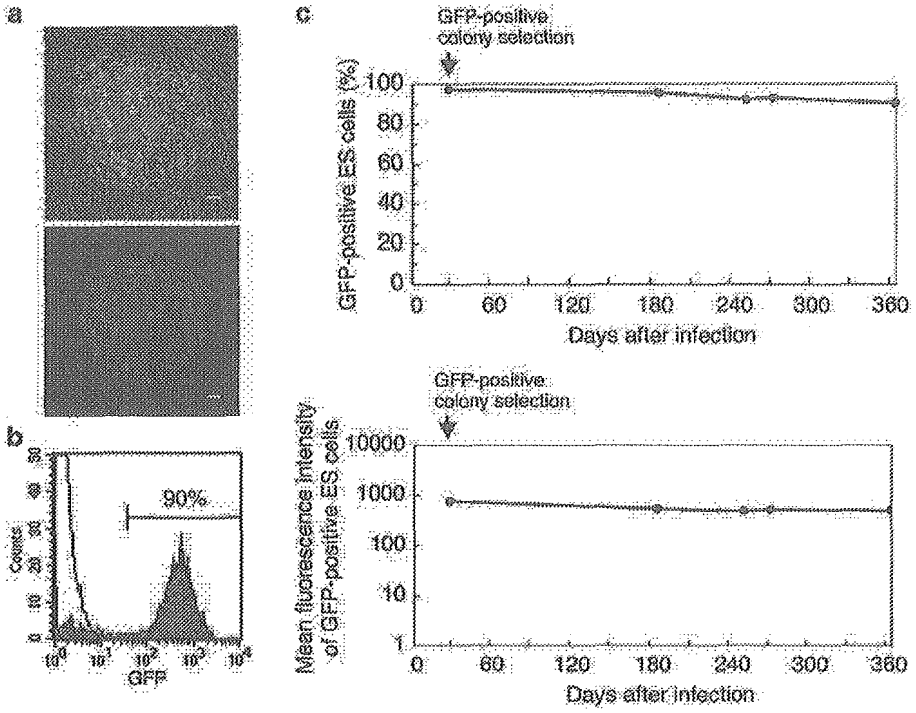

Figure 2 Stable SeV-mediated transgene expression in cynomolgus ES cells. Fluorescent ES cell colonies were plucked under a fluorescent microscope once at 1 month after infection and the cells were further propagated. (a) Phase-contrast (upper) and fluorescence (lower) images of a cynomolgus ES cell colony at day 370 after infection. Bar = 100 μm. (b) Flow cytometric analysis of SeV-infected cynomolgus ES cells at day 370 after infection (shown in green). The percentage of GFP-positive cells is indicated. Uninfected, parental cynomolgus ES cells are indicated by another line (white area). (c) The percentage of GFP-positive cells (upper) and mean fluorescence intensity per GFP-positive cell (lower) after infection with the SeV vector at 10 TU/cell are shown as a function of time (days).

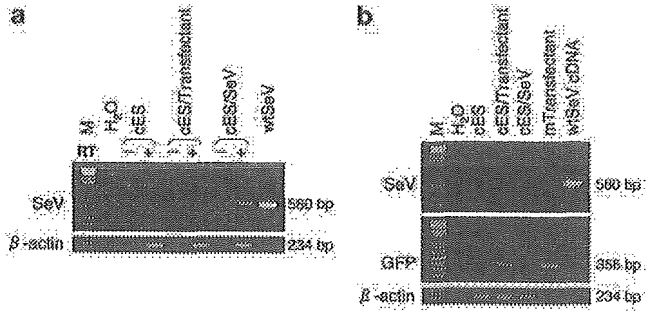

Figure 3 DNA-independent replication and transcription of SeV vector. Total cellular RNA and DNA were extracted from cynomolgus ES cells at day 284 after infection with the SeV vector. RNA-PCR (a) and DNA-PCR (b) for the SeV RNA genome or GFP sequence were conducted. The cynomolgus β-actin sequence was used as an internal control. In the RNA-PCR (a), negative results obtained without reverse transcriptase (designated RT−) confirmed that the amplified products were not derived from cellular DNA. M, 100-kb DNA ladder; cES, naive cynomolgus ES cells; cES/Transfectant, cynomolgus ES cells stably expressing the GFP gene after transfection,[33] cES/SeV, cynomolgus ES cells infected with the SeV vector; wtSeV, wild-type SeV genome; mTransfectant, a GFP-positive mouse cell line after transfection.

diluted out. (iv) The SeV vector is much less unlikely to generate wild-type virus *in vitro* or *in vivo* than oncoretroviral and lentiviral vectors, since homologous recombination between RNA genomes is very rare indeed in negative-strand RNA viruses.[19] (v) The SeV genome is not subject to cellular epigenetic modifications such as methylation, and thus it is unlikely that methylation-based silencing of transgene expression occurs.

No cytotoxic or differentiating effect on ES cells associated with the SeV infection was observed in our study. However, the wild-type SeV contains immunogenic surface proteins, hemagglutinin-neuraminidase (HN) and F proteins, which potentially induce antibody responses.[20,21] For future clinical applications, it would be desired that as many viral genes as possible are deleted from the vector backbone to permit reapplication, improve the safety, and lessen the possible toxicity of SeV vectors. To this end, we have developed a series of attenuated SeV vectors that are F gene-deleted,[6] F gene-deleted with preferable mutations,[22] M gene-deleted,[23] or have deletions of both F and M genes.[24] The modified vectors would be safer for *in vivo* use.

Ribavirin at high concentrations seems toxic to ES cells; presumably, it directly hampers viability and proliferation potential of ES cells. However, we cannot tell whether the observed toxicity is simply due to its toxicity to ES cells, as feeder cells are more highly sensitive to ribavirin than ES cells. In fact, while feeder cells died at 1 mM of ribavirin, cocultured ES cells were alive at this concentration for some time. Cynomolgus ES cells lose pluripotency and proliferation potential without feeder cells. Thus, the observed toxicity to ES cells may also be a secondary event following the injury of feeder cells. Whether the cytotoxicity is primary or secondary, it will be necessary to find modified compounds of less cytotoxicity.

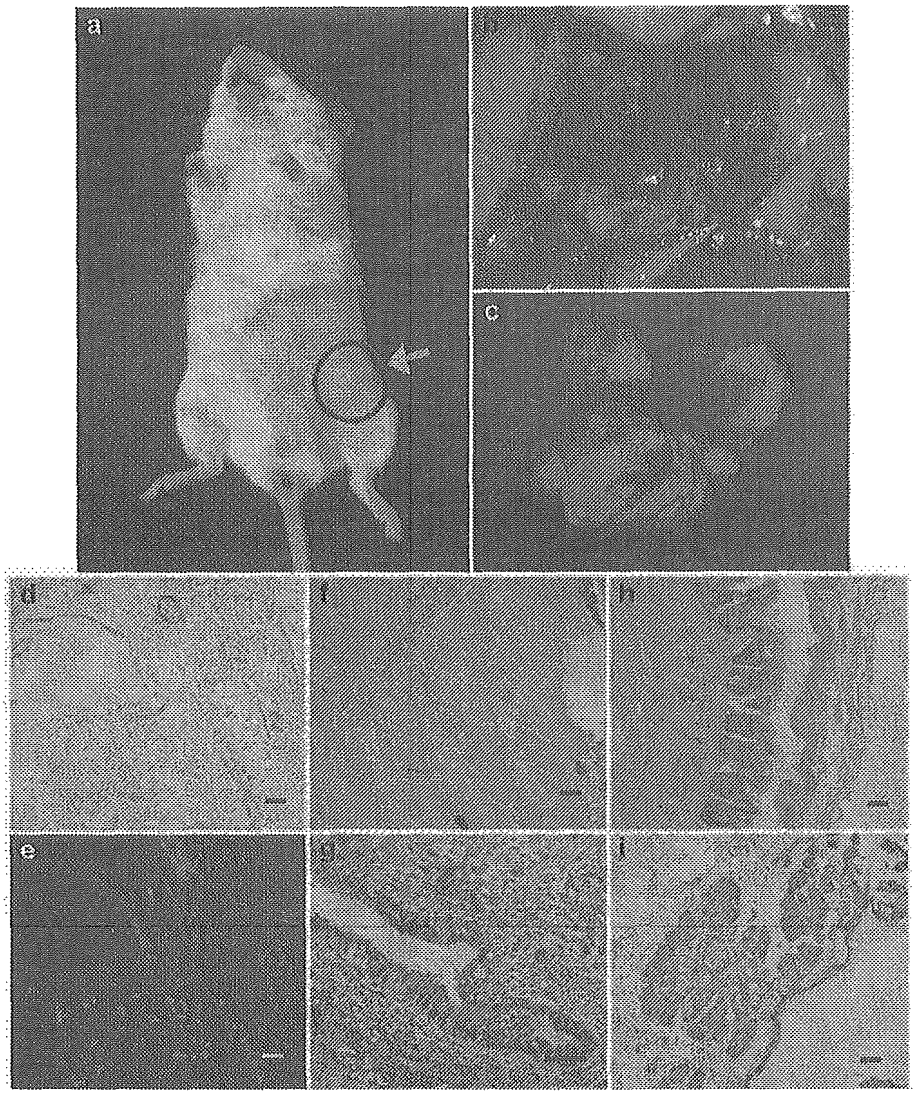

Figure 4 Pluripotency of SeV-infected cynomlgus ES cells. Tumors formed in NOD-SCID mice after inoculation of the SeV-infected cynomolgus ES cells (a). The tumor was fluorescing ((b), bright field; (c), dark field). Fluorescence was observed uniformly in the tumor under a fluorescent microscope ((d), bright field; (e), dark field). The tumor contained all three embryonic germ layer cells; cartilage (f), ciliated columnar epithelium (g), skin (h), and sebaceous gland (i) (stained with hematoxylin and eosin). Bar = 100 μm.

Materials and methods

Cell culture

Cynomolgus ES cells (CMK6) were maintained on a feeder layer of mitomycin C (Kyowa, Tokyo, Japan)-treated mouse (BALB/c) embryonic fibroblasts as described previously.[18] The culture medium consisted of Dulbecco's modified Eagle's medium (DMEM)/F12 (Invitrogen, Carlsbad, CA, USA) supplemented with 15% ES cell-qualified fetal calf serum (FCS; Invitrogen), 0.1 mM 2-mercaptoethanol (Sigma, St Louis, MO, USA), 2 mM glutamine (Invitrogen), 0.1 mM nonessential amino acids (Invitrogen), and antibiotics (100 U/ml penicillin and 100 μg/ml streptomycin, Irvine Scientific, Santa Ana, CA, USA). The ES cell colonies were routinely passaged every 3–4 days after dissociation with a combined approach of 0.25% trypsin (Invitrogen) digestion and mechanical cutting. Alkaline phosphatase staining was conducted with an Alkaline Phosphatase Chromogen Kit (Biomeda, Foster City, CA, USA). Embryoid bodies were produced by culturing ES cell aggregates in Petri dishes. LLC-MK2 cells (1×10^6) were grown in six-well plates and cultured in Eagle's minimal essential medium (Invitrogen) supplemented with 10% FCS.

Vectors

The F-defective SeV vector carrying the GFP gene was constructed as previously described.[6] The vector titer was 1.8×10^9 TU/ml determined by counting fluorescent cells after the infection of LLC-MK2 cells. Gene transfer was conducted by adding various concentrations of the SeV vector solution to culture media. After 24 h of incubation, the cells were washed twice with phosphate-buffered saline (PBS) and fresh medium was added. In some experiments, ribavirin (1-β-D-ribofuranosyl-1,2,4-triazole-3-carboxamide; Sigma) was added at various concentrations to the culture media after infection. The

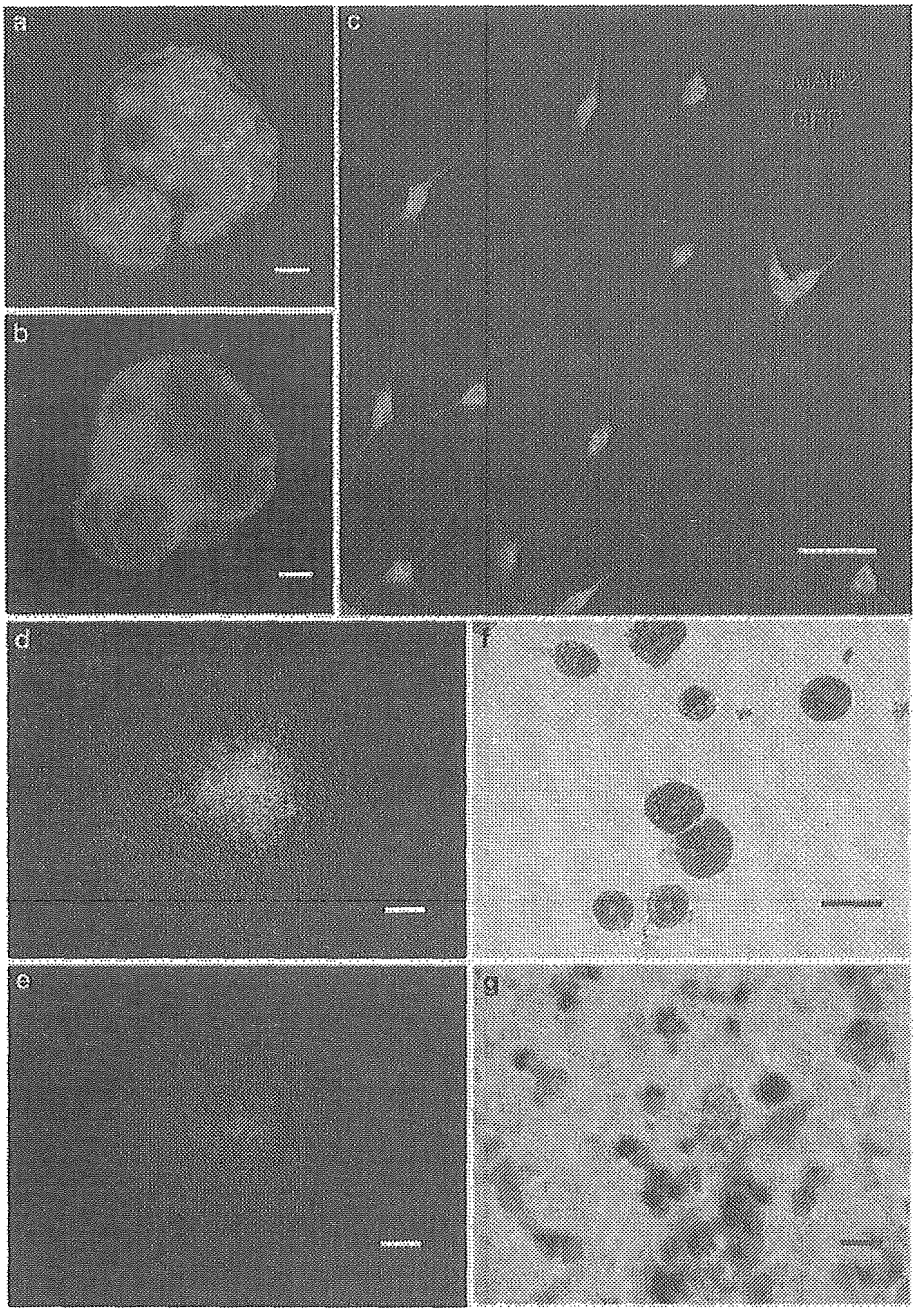

Figure 5 Stable transgene expression during differentiation. A day-20 cystic embryoid body was observed under a fluorescent phase-contrast microscope, confirming that the embryoid body was fluorescing ((a), bright field; (b), dark field). After infection with the SeV vector, fluorescent cynomolgus ES cells differentiated into neural cells. Double immunostaining with anti-GFP (green) and ant-MAP-2 (red) confirmed that differentiated neural cells expressed GFP (c). Yellow cells indicate GFP-expressing neurons. SeV-infected, fluorescent cynomolgus ES cells also differentiated into fluorescent hematopoietic cells. A clonogenic hematopoietic colony was fluorescing ((d) bright field; (e), dark field). A cytospin specimen of hematopoietic colony cells (Wright–Giemsa staining) showed that the cells were mature granulocytes (f). The infected ES cell-derived, fluorescent neutrophils were positive for NBT (stained in black (g)). Bar = 100 μm (a, b, g); 50 μm (c, f); 500 μm (d, e).

viral particles in infected cells were quantified by a hemagglutination assay as described previously.[25]

An adenovirus serotype 5-based vector carrying the GFP gene was constructed as reported.[26] It contained the cytomegalovirus (CMV) promoter, simian virus (SV)-40 intron, and SV-40 polyadenylation signal. An AAV serotype 2-based vector expressing the GFP gene under the control of the chicken β-actin promoter with the CMV immediate-early enhancer (a gift from Dr J Miyazaki) was prepared as described previously.[27] Gene transfer experiments were performed using 3.4×10^2 genome copies (g.c.)/cell of the adenoviral vector or 2.4×10^4 g.c./cell of the AAV vector. The period of exposure was 48 h.

Flow cytometry

GFP and SSEA-4 expression was analyzed on a FACScan (Becton Dickinson, Franklin Lakes, NJ, USA) using the

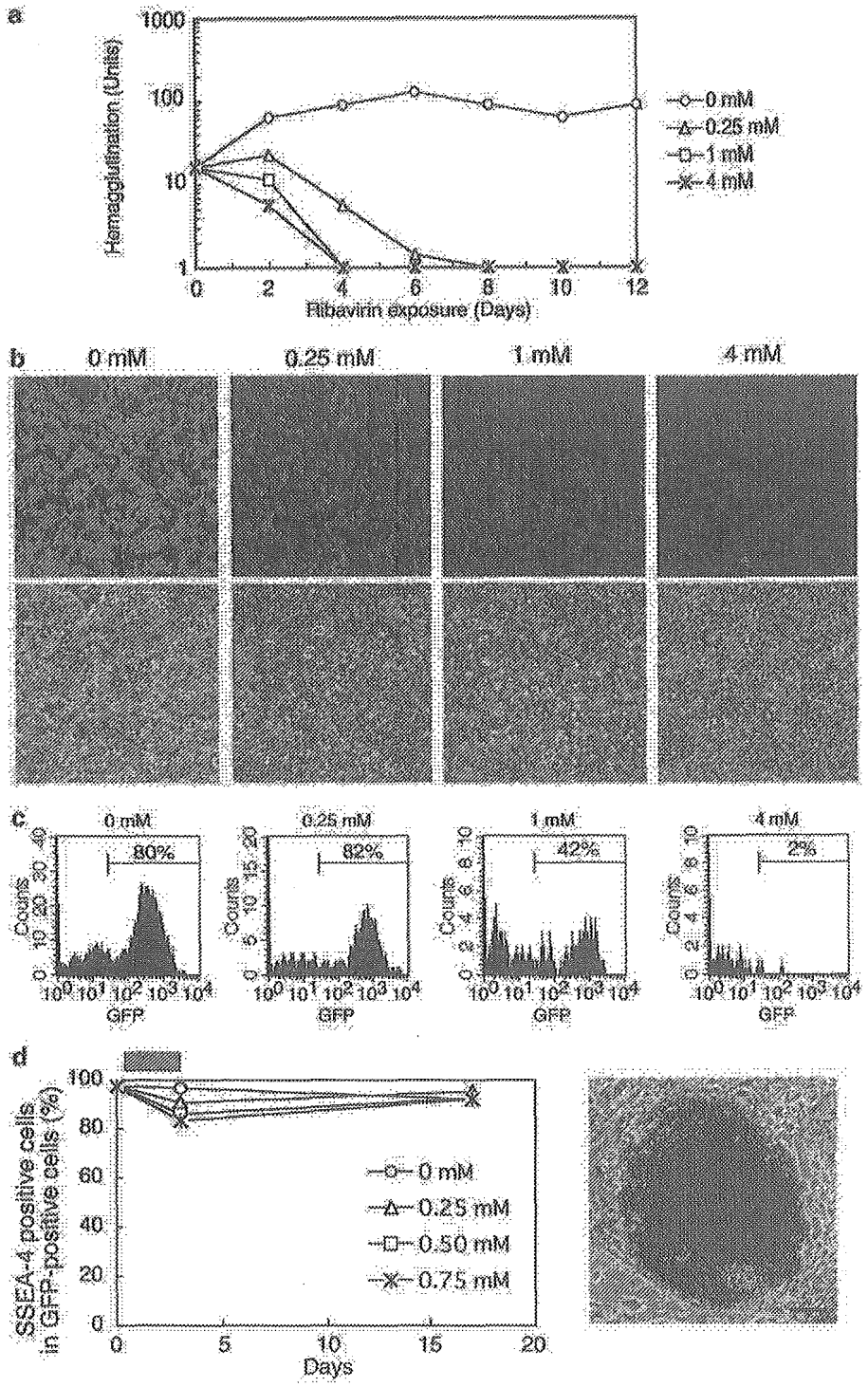

Figure 6 *Ribavirin-regulated transgene expression. (a) A rhesus kidney cell line (LLC-MK2) was infected with the SeV vector at 3 TU/cell. Ribavirin was started at various concentrations on day 2 after the infection. The formation of viral particles in the infected LLC-MK2 cells was examined by the hemagglutination assay. (b) The ribavirin-treated LLC-MK2 cells were observed under a fluorescent microscope after an 8-day exposure of ribavirin (upper, dark field; lower, bright field). (c) Ribavirin was added at various concentrations to the SeV-infected, fluorescent cynomolgus ES cells. The GFP expression was assessed by flow cytometry after a 3-day exposure of ribavirin. (d) The fractions of SSEA-4-positive ES cells were assessed by flow cytometry with anti-SSEA-4 before and after a 3-day exposure of ribavirin and are shown as a function of time (days) in the left panel. A gray bar indicates ribavirin treatment. ES cells were stained for alkaline phosphatase (in red) at day 21 after a 3-day exposure of 0.75 mM ribavirin and are shown in the right panel. Bar = 100 μm.*

CellQuest software (Becton Dickinson). For SSEA-4 staining, cells were incubated with a primary antibody, anti-SSEA-4 (MC-813-70; Chemicon, Temecula, CA, USA), and then a secondary antibody, PE-conjugated F(ab')2 fragment of rabbit anti-mouse immunoglobulins (DakoCytomation, Glostrup, Denmark). Cocultured BALB/c feeder cells could be distinguished from cynomolgus ES cells by using PE-conjugated anti-mouse

H-2d (SF1-1.1; PharMingen, San Diego, CA, USA), which does not react to cynomolgus cells but does react to BALB/c cells.

Teratoma formation

Cynomolgus ES cells (approximately 10^6 cells per site) were injected subcutaneously into the hind leg of 6- to 8-week-old nonobese diabetic/severe combined immunodeficient mice (Jackson Laboratory, Bar Harbor, ME, USA). The resulting tumors (usually 9–12 weeks after the injection) were dissected and fixed in 4% paraformaldehyde. For histological analysis, samples from the tumors were embedded in paraffin and stained with hematoxylin and eosin. To observe GFP fluorescence, samples were embedded in OTC compound (Sakura, Zoeterwoude, Netherlands), frozen, sectioned, and examined under a fluorescence microscope.

Hematopoietic differentiation

The mouse bone marrow stromal cell line OP9 was maintained in α-modified minimum essential medium (Invitrogen) supplemented with 20% FCS as described previously.[28] For induction of hematopoietic differentiation, ES cells were seeded onto a mitomycin C-treated confluent OP9 cell layer in six-well plates. Medium to support the differentiation was described elsewhere.[29] Cells at day 18 were placed in Methocult GF+ media (StemCell Technologies, Vancouver, Canada) at 1×10^4 and 1×10^5 cells per plate and clonogenic hematopoietic colonies were produced. After 14 days, individual colonies were removed and spun onto glass slides. Cells were stained with the Wright–Giemsa method. The nitro blue tetrazolium (NBT, Sigma) reduction test was performed on the cells as a granulocyte functional assay according to a previously described method.[30]

Neural differentiation

The induction of neural differentiation was carried out as described previously.[31] Day-4 embryoid bodies were plated onto tissue culture dishes and nestin-positive cells were selected in DMEM/F12 medium supplemented with 5 μg/ml of insulin (Sigma), 50 μg/ml of transferrin (Sigma), 30 nM selenium chloride (Sigma), and 5 μg/ml of fibronectin (Sigma) for 5 days. Cells were then trypsinized and plated in polyornithine-coated dishes (15 μg/ml) and expanded in N2 medium[32] supplemented with 1 μg/ml of laminin (Sigma) and 10 μg/ml of basic fibroblast growth factor (bFGF; Roche, Basel, Switzerland) for 6 days. Differentiation was induced by removal of bFGF. To confirm the neural differentiation, cells were stained with anti-human MAP-2. Briefly, cells were fixed in 4% paraformaldehyde in PBS and incubated with anti-human MAP-2 (HM-2; Sigma; diluted 1:4000) and then by Alexa Fluor 594-labeled antibody (diluted 1:500; Molecular Probe, Eugene, OR, USA). The samples were examined under a fluorescence microscope.

DNA-PCR

DNA-PCR for the SeV genome and GFP sequences was carried out as follows. DNA was extracted using the QIAamp DNA mini kits (Qiagen, Hilden, Germany) and 250 ng was used for each PCR with ExTaq (Takara, Shiga, Japan). Amplification conditions were 30 cycles of 94°C for 1 min, a variable annealing temperature (noted below) for 1 min, and 72°C for 1 min. The amplified products were run on 2% agarose gel and visualized by ethidium bromide staining. Primer sequences, annealing temperatures and product sizes were as follows: the SeV vector genome sequence: 5′-AGA GAA CAA GAC TAA GGC TAC C-3′ and 5′-ACC TTG ACA ATC CTG ATG TGG-3′ (55°C, 580 bp); the GFP sequence: 5′-CGT CCA GGA GCG CAC CAT CTT C-3′ and 5′-GGT CTT TGC TCA GGG CGG ACT-3′ (60°C, 356 bp). the cynomolgus β-actin sequence: 5′-CAT TGT CAT GGA CTC TGG CGA CGG-3′ and 5′-CAT CTC CTG CTC GAA GTC TAG GGC-3′ (60°C, 234 bp).

RNA-PCR

RNA-PCR for the SeV RNA genomic sequence was carried out as follows. Total RNA was extracted using RNA STAT-60 (Tel-Test, Friendswood, TX, USA). Reverse transcription was conducted by using Taqman reverse transcription reagents (Applied Biosystems, Foster City, CA, USA). The product (250 ng) after the reverse transcription was used for the subsequent PCR as described above.

Acknowledgements

Cynomolgus ES cells were provided by Norio Nakatsuji (Kyoto University, Kyoto, Japan), Yasushi Kondo (Tanabe Seiyaku Co. Ltd, Osaka, Japan), and Ryuzo Torii (Shiga University of Medical Science, Shiga, Japan). OP9 cells were provided by Toru Nakano (Osaka University, Osaka, Japan). We thank Yujiro Tanaka and Takayuki Asano for cultivating cynomolgus ES cells and Takeshi Hara for conducting NBT tests. We also thank Natsuko Kurosawa for technical assistance.

References

1 Thomson JA *et al.* Embryonic stem cell lines derived from human blastocysts. *Science* 1998; **282**: 1145–1147.
2 Reubinoff BE *et al.* Embryonic stem cell lines from human blastocysts: somatic differentiation *in vitro*. *Nat Biotechnol* 2000; **18**: 399–404.
3 Asano T *et al.* Highly Efficient gene transfer into primate embryonic stem cells with a simian lentivirus vector. *Mol Ther* 2002; **6**: 162–168.
4 Ma Y *et al.* High-level sustained transgene expression in human embryonic stem cells using lentiviral vectors. *Stem Cells* 2003; **21**: 111–117.
5 Gropp M *et al.* Stable genetic modification of human embryonic stem cells by lentiviral vectors. *Mol Ther* 2003; **7**: 281–287.
6 Li HO *et al.* A cytoplasmic RNA vector derived from nontransmissible Sendai virus with efficient gene transfer and expression. *J Virol* 2000; **74**: 6564–6569.
7 Yonemitsu Y *et al.* Efficient gene transfer to airway epithelium using recombinant Sendai virus. *Nat Biotechnol* 2000; **18**: 970–973.
8 Masaki I *et al.* Recombinant Sendai virus-mediated gene transfer to vasculature: a new class of efficient gene transfer vector to the vascular system. *FASEB J* 2001; **15**: 1294–1296.
9 Shiotani A *et al.* Skeletal muscle regeneration after insulin-like growth factor I gene transfer by recombinant Sendai virus vector. *Gene Therapy* 2001; **8**: 1043–1050.
10 Yamashita A *et al.* Fibroblast growth factor-2 determines severity of joint disease in adjuvant-induced arthritis in rats. *J Immunol* 2002; **168**: 450–457.

11 Ikeda Y *et al.* Recombinant Sendai virus-mediated gene transfer into adult rat retinal tissue: efficient gene transfer by brief exposure. *Exp Eye Res* 2002; **75**: 39–48.
12 Jin CH *et al.* Recombinant Sendai virus provides a highly efficient gene transfer into human cord blood-derived hematopoietic stem cells. *Gene Therapy* 2003; **10**: 272–277.
13 Crotty S *et al.* The broad-spectrum antiviral ribonucleoside ribavirin is an RNA virus mutagen. *Nat Med* 2000; **6**: 1375–1379.
14 Vo NV, Young KC, Lai MM. Mutagenic and inhibitory effects of ribavirin on hepatitis C virus RNA polymerase. *Biochemistry* 2003; **42**: 10462–10471.
15 McHutchison JG *et al.* Interferon alfa-2b alone or in combination with ribavirin as initial treatment for chronic hepatitis C. Hepatitis Interventional Therapy Group. *N Engl J Med* 1998; **339**: 1485–1492.
16 Davis GL *et al.* Interferon alfa-2b alone or in combination with ribavirin for the treatment of relapse of chronic hepatitis C. International Hepatitis Interventional Therapy Group. *N Engl J Med* 1998; **339**: 1493–1499.
17 McCormick JB *et al.* Lassa fever. Effective therapy with ribavirin. *N Engl J Med* 1986; **314**: 20–26.
18 Suemori H *et al.* Establishment of embryonic stem cell lines from cynomolgus monkey blastocysts produced by IVF or ICSI. *Dev Dyn* 2001; **222**: 273–279.
19 Spann KM, Collins PL, Teng MN. Genetic recombination during coinfection of two mutants of human respiratory syncytial virus. *J Virol* 2003; **77**: 11201–11211.
20 Tozawa H *et al.* Neutralizing activity of the antibodies against two kinds of envelope glycoproteins of Sendai virus. *Arch Virol* 1986; **91**: 145–161.
21 Tashiro M, Tobita K, Seto JT, Rott R. Comparison of protective effects of serum antibody on respiratory and systemic infection of Sendai virus in mice. *Arch Virol* 1989; **107**: 85–96.
22 Inoue M *et al.* Nontransmissible virus-like particle formation by F-deficient Sendai virus is temperature sensitive and reduced by mutations in M and HN proteins. *J Virol* 2003; **77**: 3238–3246.
23 Inoue M *et al.* A new Sendai virus vector deficient in the matrix gene does not form virus particles and shows extensive cell-to-cell spreading. *J Virol* 2003; **77**: 6419–6429.
24 Inoue M *et al.* Recombinant Sendai virus vectors deleted in both the matrix and the fusion genes: efficient gene transfer with preferable properties. *J Gene Med*, published online 5 May 2004. doi:10.1002/jgm.597.
25 Kato A *et al.* Initiation of Sendai virus multiplication from transfected cDNA or RNA with negative or positive sense. *Genes Cells* 1996; **1**: 569–579.
26 Okada T *et al.* Efficient directional cloning of recombinant adenovirus vectors using DNA–protein complex. *Nucleic Acids Res* 1998; **26**: 1947–1950.
27 Okada T *et al.* Adeno-associated viral vector-mediated gene therapy of ischemia-induced neuronal death. *Methods Enzymol* 2002; **346**: 378–393.
28 Nakano T, Kodama H, Honjo T. Generation of lymphohematopoietic cells from embryonic stem cells in culture. *Science* 1994; **265**: 1098–1101.
29 Li F *et al.* Bone morphogenetic protein 4 induces efficient hematopoietic differentiation of rhesus monkey embryonic stem cells *in vitro*. *Blood* 2001; **98**: 335–342.
30 Sekhsaria S *et al.* Peripheral blood progenitors as a target for genetic correction of $p47^{phox}$-deficient chronic granulomatous disease. *Proc Natl Acad Sci USA* 1993; **90**: 7446–7450.
31 Lee SH *et al.* Efficient generation of midbrain and hindbrain neurons from mouse embryonic stem cells. *Nat Biotechnol* 2000; **18**: 675–679.
32 Johe KK *et al.* Single factors direct the differentiation of stem cells from the fetal and adult central nervous system. *Genes Dev* 1996; **10**: 3129–3140.
33 Takada T *et al.* Monkey embryonic stem cell lines expressing green fluorescent protein. *Cell Transplant* 2002; **11**: 631–635.

Journal of Thrombosis and Haemostasis, 3: 909–914

REVIEW ARTICLE

Molecular mechanisms of age-related regulation of genes

K. KURACHI and S. KURACHI
Age Dimension Research Center, National Institute of Advanced Industrial Science and Technology, Tsukuba, Ibaraki, Japan

To cite this article: Kurachi K, Kurachi S. Molecular mechanisms of age-related regulation of genes. *J Thromb Haemost* 2005; 3: 909–14.

Introduction

Age is a critical risk factor for many diseases such as thrombosis, cardiovascular diseases, cerebral vascular diseases, diabetes, cancer and Alzheimer's disease [1–10]. Although its importance has been shown clearly by many epidemiological studies, literally nothing is known about its molecular mechanisms of action.

Physiological systems are controlled by homeostatic mechanisms, maintaining them within small tolerable fluctuation ranges. Various internal or external insults, stresses or pathological conditions affect the homeostatic conditions. Importantly, homeostatic conditions of physiological systems are not constant with age, but continue changing slowly with age [11–13]. Such physiological changes may play a critical role either additively or synergistically in the initiation and development of many age-dependent diseases.

To explore the little-understood molecular mechanisms of age-dimension homeostasis, we first focused our study on the blood coagulation system, our model physiological system for the study (Fig. 1). This led to the first discovery of the molecular mechanisms of age-related gene regulation and therefore of homeostatic regulation of physiological systems. In this article, we review recent advances in this newly emerging research field.

Blood coagulation system and age

The complex formation of factor VII with tissue factor, which becomes available upon tissue injury, initiates blood coagulation [14] (Fig. 1). This initial reaction triggers cascades of reactions involving nearly 20 pro- and anticoagulant factors, resulting in a sufficient amount of stable fibrin clot production in a matter of minutes. Most cascade steps of this system are of proteolytic reactions in combination with increasing levels of plasma concentration of procoagulant factors as they go downstream, thus making blood coagulation an extremely efficient amplification system. In healthy individuals, blood coagulation activity makes a rapid increase during the perinatal stage and reaches a level similar to that of young adults at around weaning, followed by a gradual and continuous increase with age [15–19]. As demonstrated by epidemiological evidence [11,17,18,20], this appears to be due to an age-dependent increase in an imbalance between procoagulant activity and anticoagulant activities. Plasma concentration and/or activity of most known procoagulant factors (shown with arrows in Fig. 1) increase with age, whereas anticoagulant factors such as antithrombin (ATIII), TFPI and protein C, and profibrinolytic factors including plasminogen and tPA do not increase with age or, in some cases, even decrease slightly with age [20–22]. Importantly, PAI-1, an inhibitor of tPA which catalyzes plasminogen activation to plasmin, also increases its plasma concentration with age [22], thus resulting in an enhancement of procoagulant tendency. Together, this evidence indicates that as age proceeds, the balance between the overall procoagulant activity including the antifibrinolytic activity and that of the anticoagulant activity combined with the fibrinolytic activity tips toward the procoagulant state. In combination with various environmental conditions, including diet consumed, such an imbalance may contribute to an increased thrombotic tendency, particularly in elderly people [16–21,23,24].

Circulatory levels of human factor IX (hFIX), a key coagulation factor, significantly increase with advancing age in normal human populations [11,16,25]. In contrast, circulatory levels of human PC (hPC), a key factor in the potent anticoagulant protein C pathway, show a stable pattern with only marginal, if any, age-associated fluctuations [11,16,21]. Therefore, we considered that our studies on the age-related regulatory mechanisms of hFIX and hPC genes may provide us with critical information on the fundamental molecular mechanisms involved in the age-dimension homeostasis of gene expression.

Assay systems

Natural gene sizes of hFIX and hPC are approximately 40 and 13 kb pairs, respectively. To make experimental manipulations feasible, we constructed a series of their minigenes [26–31] (Fig. 2). After verifying with HepG2 cells for appropriate construction of these minigene vectors and their expression activities, all the minigene vectors were subjected to systematic

Correspondence: Kotoku Kurachi, Age Dimension Research Center, National Institute of Advanced Industrial Science and Technology, 1-1-1, Higashi, Tsukuba, Ibaraki, 305-8566, Japan.
Tel.: +81 298 61 6528; fax: +81 298 61 2788; e-mail: k.kurachi@aist.go.jp

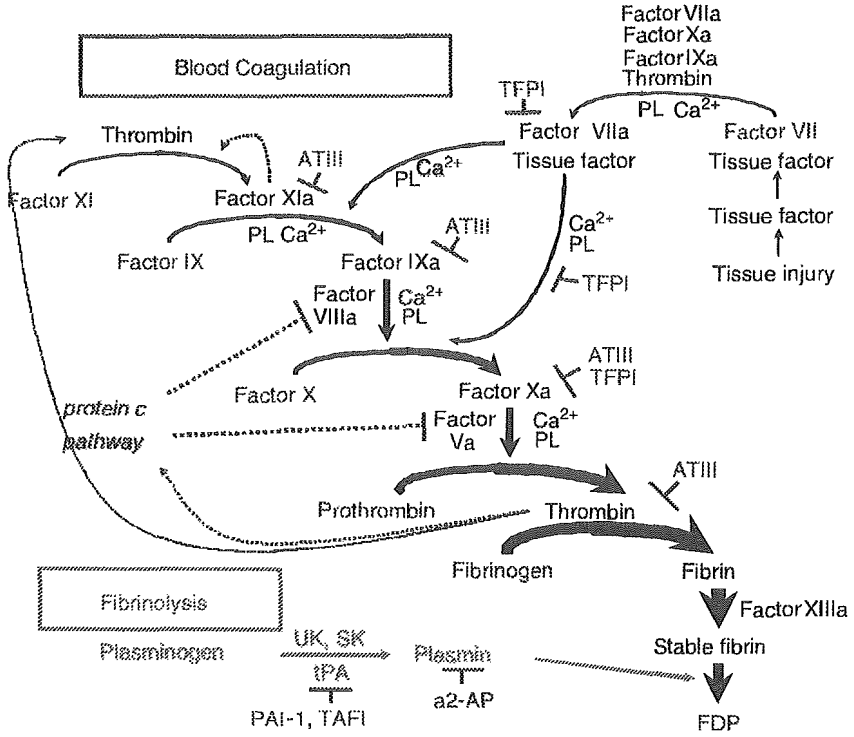

Fig. 1. Blood coagulation and fibrinolysis cascades. Procoagulation factors, shown with connecting arrows, increase their plasma concentrations or activities, while anticoagulation factors shown with T bars and profibrinolysis factors do not. Here, simplified blood coagulation and fibrinolysis cascades are shown to illustrate the essential relationships of factors involved.

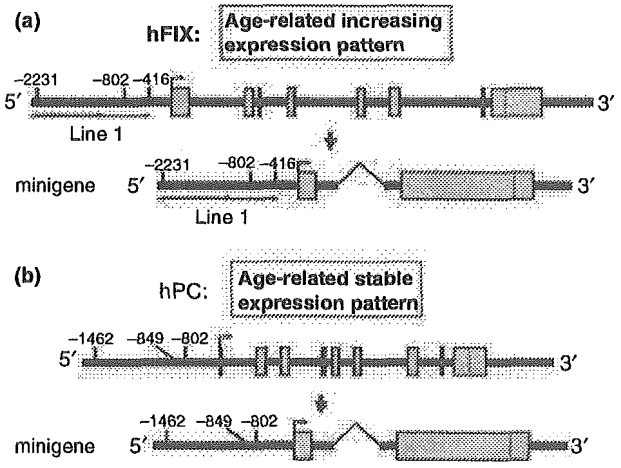

Fig. 2. Basic frameworks of minigene constructs of hFIX (a) and hPC (b) genes. hFIX and hPC genes are represented by horizontal lines with exons shown as fattened portions. Relative positions of LINE-1 (retrotransposable element)-derived sequences of the hFIX gene are shown with overlapped horizontal arrows. Exemplary minigenes are shown.

construction of transgenic mice. Circulatory levels of hFIX or hPC produced in individual transgenic animals were then monitored biweekly or monthly as needed for their life spans using serum samples and hFIX or hPC-specific enzyme-linked immunosorbent assays (ELISA).

Characteristics of the mouse blood coagulation system are similar to those of the human system, and we showed that age-related expression patterns of FIX and PC genes, age-related increase or stable, respectively, are also similar to those of the human counterparts [26,27]. This similarity justified mice as our animal model for analyzing the age-dimension homeostasis of gene expression.

Discovery of the first age-related regulatory mechanisms of gene expression

After systematic analyses of many lines of hFIX minigenes in transgenic mice, we identified two genetic elements, ASE and AIE (renamed from the initial names, AE5′- and AE3′, respectively; see [26,27]) to be essential for generating age-related stable and increase patterns, respectively, of hFIX gene expression [26] (Fig. 3). ASE is located to a small 5′ upstream region, nucleotide (nt) −802 to nt −784, of the hFIX gene sequence by footprinting assay and electrophoretic mobility shift assay (EMSA). ASE has a nucleotide core sequence, GAGGAAG, matching the Ets element consensus sequence (GGAAT) for the binding of Ets family transcriptional factors such as PEA-3 [32,33]. AIE, an element necessary for age-related increase in gene expression, was identified in the middle of the hFIX 3′-untranslated region (UTR) [26]. AIE is composed of a 102 base pair (bp) dinucleotide repeat (mostly AT, GT, CA), and has the potential to form three distinct stem loop structures in its RNA form [28]. Mouse factor IX (mFIX) shows an age-related increase in both its plasma level and gene expression level in the liver [34,35], and its gene contains an

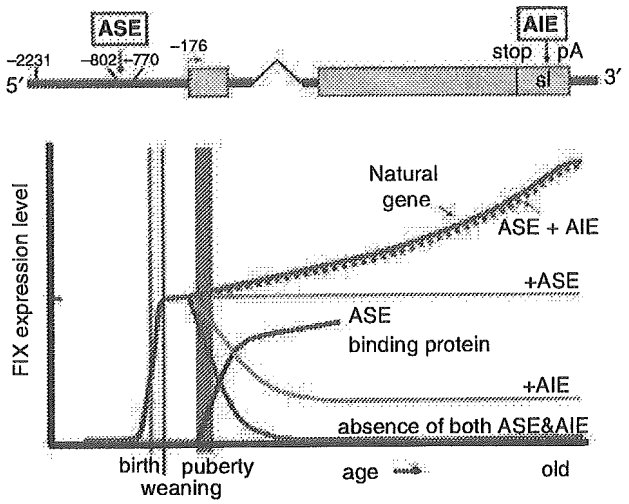

Fig. 3. The age-regulatory mechanisms of the hFIX gene. Relative positions of genetic components, ASE and AIE are shown at the top. Age-related patterns of circulatory hFIX levels for minigenes with or without ASE and/or AIE are shown schematically. These patterns are essentially parallel to those of the hFIX mRNA levels in the liver tissues.

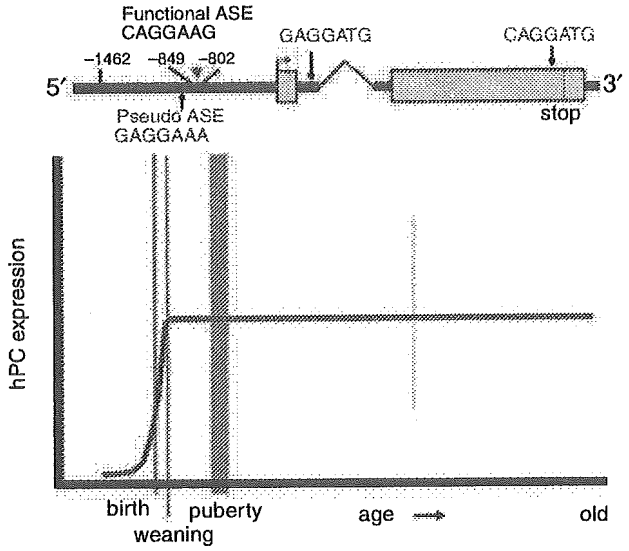

Fig. 4. Mechanisms of age-related regulation of the hPC gene. The age-stable expression pattern of the hPC gene due to the presence of its functional ASE (CAGGAAG) and absence of any AIE is shown in the lower panel. Relative positions of the similar Ets consensus sequences but with no age-regulatory function are also shown with thin letters.

ASE sequence identical to the functional ASE in the hFIX gene and an AIE-like stretch of 106 bp dinucleotide repeats in the mFIX 3′-UTR [36]. Through testing in transgenic mice, we showed that the mFIX repeat actually functions as an active AIE [27]. These studies demonstrated that the age-related increase in expression of the FIX gene is regulated by a combination of two unique genetic elements, ASE and AIE (Fig. 3). In the absence of ASE, minigenes with or without AIE show an age-unstable hFIX gene expression pattern with a rapid decline in expression over the puberty period, and in the subsequent 3–4 months decline to low but stable levels or very low basal levels, respectively. In the presence of both ASE and AIE, the age-related expression increase pattern of the hFIX gene is reproduced. Importantly, the clearance rate ($t_{½}$) of human factor IX from the blood circulation does not change significantly over age [26,27]. This is the first discovery of the age-related regulatory mechanisms of gene expression.

What molecular mechanisms function in regulation of age-stable hPC gene expression? As mentioned above, we first confirmed that the mouse PC gene expression pattern is age-stable, similar to that of the hPC gene [27]. hPC and hFIX share significant similarities in protein structure and therefore coding regions of their genes, whereas the 5′-flanking regions and 3′-UTRs are grossly dissimilar, indicating unrelated evolutional origins [28,30,37,38]. For example, we have shown previously that the 5′-flanking region of the hFIX gene beyond approximately nt −350, including the region containing ASE, was derived from the retrotransposable element LINE-1 inserted into the 5′ UTR [38] (Fig. 2). In contrast, the 5′-flanking region of the hPC gene has no LINE-1 or its remnant sequences, indicating that no retrotransposition events took place. In addition, 3′-UTR sequences of hFIX and hPC genes share no similarity except the minimal local sequences required for polyadenylation at the 3′ end regions. The 3′-UTR sequence of the hFIX gene is about 1.4 kb in length, whereas that of the hPC gene is only 295 bp, and has no AIE or AIE-like element or dinucleotide repeats [28,30]. These differences between the hFIX and hPC genes correlated with the dissimilarities in their age-related expression patterns as well as tissue-specific expression patterns.

As shown in Fig. 4, age-related stable patterns of circulatory hPC were observed with transgenic mice carrying hPC minigene −1462hPCm1 or −849hPCm1, recapitulating the natural age-stable expression patterns of mPC and hPC genes [27].

These minigenes had 5′ flanking sequences where their promoter regions are contained, extending to either nt −1462 or −849, respectively. However, expression patterns of minigene −802hPCm1 were age-unstable, thus identifying CAGGAAG, present in the region spanning nt −832 to nt −826, as the functional hPC ASE responsible for the age-stable expression pattern of the hPC gene. The functional ASE sequences of both hPC and hFIX genes bind the same liver nuclear protein, but other sequences do not function even with their close similarity, as shown by EMSA DNA-protein binding assays [27]. It is important to emphasize that hFIX ASE and hPC ASE have independent evolutionary origins. hFIX ASE was derived through mutational changes of a LINE-1 sequence inserted originally by a retrotransposition, while the hPC gene never experienced LINE-1 retrotransposition, and its ASE was derived through a different mechanism. This is a case of function-driven convergent evolution generating a critical genetic element required for homeostatic regulation of genes.

Pseudo-ASE (GAGGAAA) present at the 5′ upstream close to the functional hPC ASE binds a nuclear protein different

from that bound to the functional ASEs, and it does not function as an age-related regulatory element [27]. Furthermore, two other ASE-like known Ets consensus elements, one in the first intron (GAGGATG) and the other in the last exon (CAGGATG), bind an identical nuclear protein, but again different from the protein which binds to the functional ASEs (G/CAGGAAG). These elements also do not function for age-related gene regulation. Together, these results indicate that specific single base differences in the motif G/CAGGAA/TG/A facilitate strictly selective binding of specific Ets family nuclear proteins, thus conferring distinctly different functions. As we tested in transgenic mice, hFIX ASE could functionally substitute hPC ASE in the regulation of hPC gene expression [27]. ASE functions through binding a unique, probably Ets, family transcription factor. Its identification and characterization studies are in progress.

The hPC gene does not have any AIE-like element. However, as demonstrated by animal testing with minigene −1462hPCm1/AIE, which contains a unit of hFIX AIE, the age-stable expression pattern of hPC was dramatically changed to an age-related increase pattern, similar to that of the hFIX gene [27]. The mechanism of action of AIE remains to be established. These findings, together with other observations, support the functional universality of ASE and AIE. Animal testing of the mouse gene counterpart of the hFIX AIE in combination with hPC ASE has proved its functionality. Thus, the molecular mechanisms involving ASE and AIE function across different species, at least within human and mouse physiologies.

Through differential or combined usages of ASE and AIE most, if not all, anti- or procoagulation factor genes may achieve age-related increase or stable gene expression patterns, respectively. Our observations that there are no significant differences in the rate of protein clearance from the circulation between young and old animals, either for hFIX or hPC, support this further [26,27]. Together, these observations explain how the age-related increase pattern of the overall blood coagulation activity is generated (Fig. 5). Nature may also use the mechanisms for many other genes involved in different physiological systems for their age-related regulation. Further studies in this regard are under way.

Development of age-dimension technology

New knowledge of the molecular mechanisms of age-dimension homeostasis allows us to develop a new research field, age-dimension technology (ADT). Through manipulating ASE and AIE activities, for instance, by using new drugs designed to affect the functions of ASE and/or AIE, we may be able to modify gene expression along the age axis, thus leading to the development of novel preventive and therapeutic methods for age-related diseases. Some anticipated examples of ADT applications may include the following.

One of the challenging difficulties facing the current efforts in developing effective and safe gene therapy approaches is how to secure a long-term effective gene expression *in vivo* after the initial single procedure of gene delivery without repeating it.

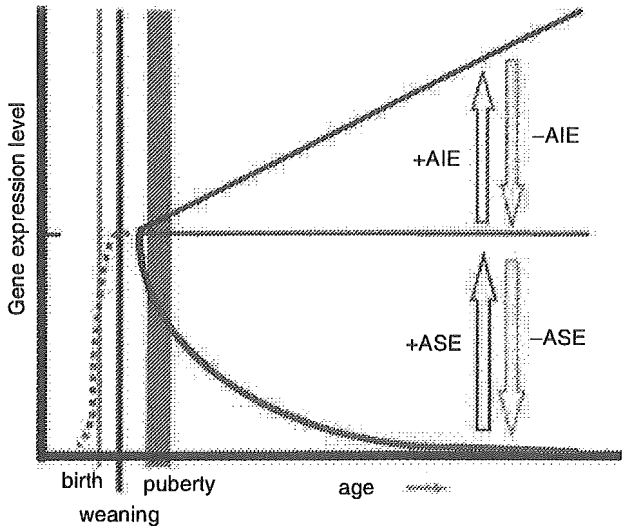

Fig. 5. The first molecular mechanisms of age-related regulation of genes and the principle of ADT. Functions of ASE and AIE in age-related regulation of gene expression are shown schematically. ASE is required for stabilization of gene expression at the prepubertal level, while AIE in the presence of ASE is responsible for age-related increase in gene expression. AIE requires the presence of ASE for its optimal function. If AIE, but not ASE is removed (shown as −AIE), gene expression is stabilized and in addition, if ASE is also removed (shown as −ASE), gene expression becomes unstable in relation to the age-axis. These findings support the possibility for developing age-related gene manipulation technology (ADT).

ADT, which allows manipulation of expression vectors with ASE and AIE, has the great potential to make it feasible, generating optimal gene delivery systems.

Another example of ADT application is described as follows. During our studies involving a large number of transgenic mice, we found that animals overexpressing hFIX at higher than certain levels (approximately 1500 ng mL^{-1} serum) die at young ages as early as 3–5 months, while control animals or animals expressing hFIX at low levels (at less than 200 ng mL^{-1} levels) live a normal life span as expected [39] (Fig. 6). In these transgenic animals, hFIX produced was additive to the mouse intrinsic FIX.

Analyses of animals dying at much younger ages than the expected age showed thrombi present in blood vessels of various tissues including the brain, lungs and heart. Some animals developed myocardial fibrosis in the left ventricle presumably induced by thrombotic occlusions of blood vessels, thus mimicking a type of human myocardial infarction. These findings indicated that even a relatively small elevation in the circulatory level of FIX, which occupies a position in the middle phase of the blood coagulation cascade, significantly shifts the blood coagulation–anticoagulation balance toward prothrombosis. Such a thrombotic tendency, however, may be eliminated effectively by suppressing the AIE function, for instance, by designing a drug antagonistic to AIE, while keeping the ASE function intact, ensuring the needed coagulation activity.

In summary, we have discovered the very first molecular mechanisms of age-related gene regulation, explaining the

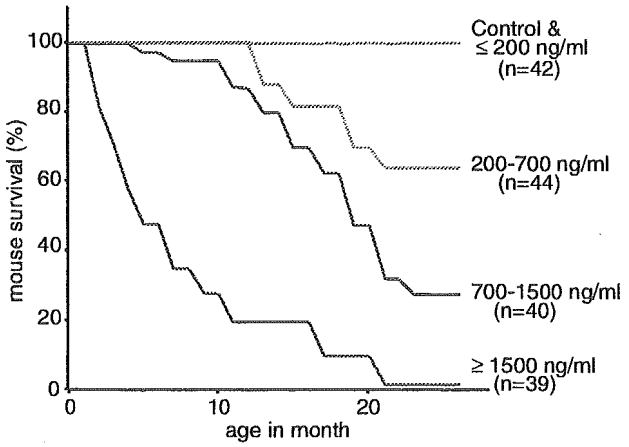

Fig. 6. Kaplan–Meier plot of transgenic mouse survival (vertical axis), level of hFIX expression and age (horizontal axis). Modified from Ameri *et al.* [39].

basic mechanisms of the age-dimension homeostasis of the blood coagulation system. This has also opened the door for discovering novel molecular mechanisms in action for age-related homeostasis of many other physiological systems.

References

1 White RH. The epidemiology of venous thromboembolism. *Circulation* 2003; **107**: 4–8.
2 Anderson FA Jr, Spencer FA. Risk factors for venous thromboembolism. *Circulation* 2003; **107**: 9–16.
3 Lusis AJ. Atherosclerosis. *Nature* 2000; **407**: 233–41.
4 Lakatta EG, Levy D. Arterial and cardiac aging: major shareholders in cardiovascular disease enterprises: part I. Aging arteries: a 'set up' for vascular disease. *Circulation* 2003; **107**: 139–46.
5 Lakatta EG, Levy D. Arterial and cardiac aging: major shareholders in cardiovascular disease enterprises: part II. The aging heart in health: links to heart disease. *Circulation* 2003; **107**: 346–54.
6 Ariesen MJ, Claus SP, Rinkel GJ, Algra A. Risk factors for intracerebral hemorrhage in the general population: a systematic review. *Stroke* 2003; **34**: 2060–5.
7 Petersen KF, Befroy D, Dufour S, Dziura J, Ariyan C, Rothman DL, DiPietro L, Cline GW, Shulman GI. Mitochondrial dysfunction in the elderly: possible role in insulin resistance. *Science* 2003; **300**: 1140–2.
8 DePinho RA. The age of cancer. *Nature* 2000; **408**: 248–54.
9 Morrison JH, Hof PR. Life and death of neurons in the aging brain. *Science* 1997; **278**: 412.
10 Bartzokis G. Age-related myelin breakdown: a developmental model of cognitive decline and Alzheimer's disease. *Neurobiol Aging* 2004; **25**: 5–18.
11 Lowe GD, Rumley A, Woodward M, Morrison CE, Philippou H, Lane DA, Tunstall-Pedoe H. Epidemiology of coagulation factors, inhibitors and activation markers: the Third Glasgow MONICA Survey. I. Illustrative reference ranges by age, sex and hormone use. *Br J Haematol* 1997; **97**: 775–84.
12 Ershler WB, Keller ET. Age-associated increased interleukin-6 gene expression, late-life diseases, and frailty. *Annu Rev Med* 2000; **51**: 245–70.
13 Linton PJ, Dorshkind K. Age-related changes in lymphocyte development and function. *Nat Immunol* 2004; **5**: 133–9.
14 Dahlback B. Blood coagulation. *Lancet* 2000; **355**: 1627–32.
15 Andrew M, Vegh P, Johnston M, Bowker J, Ofosu F, Mitchell L. Maturation of the hemostatic system during childhood. *Blood* 1992; **80**: 1998–2005.
16 Mari D, Mannucci PM, Coppola R, Bottasso B, Bauer KA, Rosenberg RD. Hypercoagulability in centenarians: the paradox of successful aging. *Blood* 1995; **85**: 3144–9.
17 Conlan MG, Folsom AR, Finch A, Davis CE, Sorlie P, Marcucci G, Wu KK. Associations of factor VIII and von Willebrand factor with age, race, sex, and risk factors for atherosclerosis: the Atherosclerosis Risk in Communities (ARIC) Study. *Thromb Haemost* 1993; **70**: 380–5.
18 Balleisen L, Bailey J, Epping PH, Schulte H, van de Loo J. Epidemiological study on factor VII, factor VIII and fibrinogen in an industrial population. I. Baseline data on the relation to age, gender, body-weight, smoking, alcohol, pill-using, and menopause. *Thromb Haemost* 1985; **54**: 475–9.
19 Wilkerson WR, Sane DC. Aging and thrombosis. *Semin Thromb Hemost* 2002; **28**: 555–68.
20 Conlan MG, Folsom AR, Finch A, Davis CE, Marcucci G, Sorlie P, Wu KK. Antithrombin III: associations with age, race, sex and cardiovascular disease risk factors. The Atherosclerosis Risk in Communities (ARIC) Study Investigators. *Thromb Haemost* 1994; **72**: 551–6.
21 Bauer KA, Weiss LM, Sparrow D, Vokonas PS, Rosenberg RD. Aging-associated changes in indices of thrombin generation and protein C activation in humans. Normative Aging Study. *J Clin Invest* 1987; **80**: 1527–34.
22 Takada Y, Takada A. Plasma levels of t-PA free PAI-1 and a complex of t-PA with PAI-1 in human males and females at various ages. *Thromb Res* 1989; **55**: 601–9.
23 Ofosu FA, Craven S, Dewar L, Anvari N, Andrew M, Blajchman MA. Age-related changes in factor VII proteolysis *in vivo*. *Br J Haematol* 1996; **94**: 407–12.
24 Hirsh J, Fuster V, Ansell J, Halperin JL. American Heart Association/American College of Cardiology Foundation guide to warfarin therapy. *Circulation* 2003; **107**: 1692–711.
25 Sweeney JD, Hoernig LA. Age-dependent effect on the level of factor IX. *Am J Clin Pathol* 1993; **99**: 687–8.
26 Kurachi S, Deyashiki Y, Takeshita J, Kurachi K. Genetic mechanisms of age regulation of human blood coagulation factor IX. *Science* 1999; **285**: 739–43.
27 Zhang K, Kurachi S, Kurachi K. Genetic mechanisms of age regulation of protein C and blood coagulation. *J Biol Chem* 2002; **277**: 4532–40.
28 Yoshitake S, Schach BG, Foster DC, Davie EW, Kurachi K. Nucleotide sequence of the gene for human factor IX (antihemophilic factor B). *Biochemistry* 1985; **24**: 3736–50.
29 Miao CH, Ho WT, Greenberg DL, Davie EW. Transcriptional regulation of the gene coding for human protein C. *J Biol Chem* 1996; **271**: 9587–94.
30 Foster DC, Yoshitake S, Davie EW. The nucleotide sequence of the gene for human protein C. *Proc Natl Acad Sci USA* 1985; **82**: 4673–7.
31 Kurachi S, Hitomi Y, Furukawa M, Kurachi K. Role of intron I in expression of the human factor IX gene. *J Biol Chem* 1995; **270**: 5276–81.
32 Xin J-H, Cowie A, Lachance P, Hassell JA. Molecular cloning and characterization of PEA3, a new member of the Ets oncogene family that is differentially expressed in mouse embryonic cells. *Genes Dev* 1992; **6**: 481–96.
33 Chotteau-Lelievre A, Desbiens X, Pelczar H, Defossez P-A, Launoit Y. Differential expression patterns of the PEA3 group transcription factors through murine embryonic development. *Oncogene* 1997; **15**: 937–52.
34 Yao S-N, DeSilva AH, Kurachi S, Samuelson LC, Kurachi K. Characterization of a mouse factor IX cDNA and developmental

regulation of the factor IX gene expression in liver. *Thromb Haemost* 1991; **65**: 52–8.

35 Kurachi S, Hitomi E, Kurachi K. Age and sex dependent regulation of the factor IX gene in mice. *Thromb Haemost* 1996; **76**: 965–9.

36 Wu S-M, Stafford DW, Ware J. Deduced amino acid sequence of mouse blood-coagulation factor IX. *Gene* 1990; **86**: 275–8.

37 Salier J-P, Hirosawa S, Kurachi K. Functional characterization of the 5′-regulatory region of human factor IX gene. *J Biol Chem* 1990; **265**: 7062–8.

38 Hsu W, Kawamura S, Fountaine J-M, Kurachi K, Kurachi S. Organization and significance of LINE-1-derived sequences in the 5′ flanking region of the factor IX gene. *Thromb Haemost* 1999; **82**: 1782–3.

39 Ameri A, Kurachi S, Sueishi K, Kuwahara M, Kurachi K. Myocardial fibrosis in mice with overexpression of human blood coagulation factor IX. *Blood* 2003; **101**: 1871–3.

Effect of Hydrodynamics-Based Gene Delivery of Plasmid DNA Encoding Interleukin-1 Receptor Antagonist-Ig for Treatment of Rat Autoimmune Myocarditis

Possible Mechanism for Lymphocytes and Noncardiac Cells

Hui Liu, MD; Haruo Hanawa, MD; Tsuyoshi Yoshida, MD; Raafat Elnaggar, MD; Manabu Hayashi, MD; Ritsuo Watanabe, MD; Ken Toba, MD; Kaori Yoshida, BS; He Chang, MD; Yuji Okura, MD; Kiminori Kato, MD; Makoto Kodama, MD; Hiroki Maruyama, MD; Junichi Miyazaki, MD; Mikio Nakazawa, PhD; Yoshifusa Aizawa, MD

Background—Interleukin-1 (IL-1) is a powerful and important cytokine in myocarditis. The purpose of this study was to evaluate the effect and possible mechanism of hydrodynamics-based delivery of the IL-1 receptor antagonist (IL-1RA)-immunoglobulin (Ig) gene for treatment of rat experimental autoimmune myocarditis (EAM).

Methods and Results—On the day after immunization, rats were transfected with either pCAGGS encoding IL-1RA-Ig or pCAGGS encoding Ig alone. On day 17, IL-1RA-Ig gene therapy was effective in controlling EAM, as monitored by a decreased ratio of heart weight to body weight, reduced myocarditis areas, reduced gene expression of atrial natriuretic peptide in hearts, and improved cardiac function in echocardiographic and hemodynamic parameters. Examination of the expression of IL-1–related genes in purified cells from EAM hearts suggested that ectopic IL-1RA-Ig–acting target cells were $\alpha\beta$T cells and noncardiomyocytic noninflammatory cells such as fibroblasts, smooth muscle cells, and endothelial cells. Therefore, we examined the effect of serum containing IL-1RA-Ig on the expression of immune-relevant genes within noncardiomyocytic cells cultured from EAM hearts or concanavalin A–stimulated lymphocytes derived from lymph nodes in EAM-affected rats. The expression of immunologic molecules (prostaglandin E synthase, cyclooxygenase-2, and IL-1β) in cultivated noncardiomyocytic cells and Th1 cytokines (IL-2 and IFN-γ) in lymphocytes was significantly decreased by the serum containing IL-1RA-Ig.

Conclusions—EAM was suppressed by hydrodynamics-based delivery of plasmid DNA encoding IL-1RA-Ig. In addition, IL-1RA-Ig suppressed gene expression of prostaglandin synthases and IL-1 in noncardiomyocytic cells and Th1 cytokines in lymphocytes. (***Circulation.*** **2005;111:1593-1600.)**

Key Words: cardiomyopathy, dilated ■ cytokines ■ sialoglycoproteins ■ myocarditis ■ prostaglandins

Rat experimental autoimmune myocarditis (EAM) resembles human giant cell myocarditis,[1] and recurrent forms lead to dilated cardiomyopathy.[2] Histopathological investigation showed that CD11b$^+$ cells (macrophages, dendritic cells, granulocytes) and CD4$^+$ T cells infiltrated the heart, which severely injured cardiomyocytes in the acute stage, followed by fibrosis in the heart.[3] Various cytokines have been found in EAM-affected hearts.[4]

Interleukin-1 (IL-1), formerly known as lymphocyte activating factor, is an important inflammatory cytokine produced by monocytes, macrophages, dendritic cells, B cells, or NK cells.[5,6] There are 2 structurally distinct forms of IL-1, IL-1α and IL-1β, which are both potent stimulators of target cells.[5,7] IL1-β, which has a signal peptide and is excreted from cells, is important for regional inflammation.[8] The IL-1 receptor (IL-1R) is divided into 2 structurally distinct forms, namely IL-1 receptor I (IL-1RI) and II (IL-1RII). IL-1RI expressed on T cells and fibroblasts among other cell types,[9] when bound to IL-1, forms heterocomplexes with IL-1 receptor accessory protein (IL-1Racp) and thereby transduces intracellular signals.[10] However, IL-1RII consisting of IL-1 binding portion, a single transmembrane region, and a shorter cytoplasmic domain cannot transduce signals and acts as a decoy target.[11] On the other hand, there are 2 structurally distinct forms of IL-1 receptor antagonist (IL-1RA) made by alternative splicing: secreted IL-1RA (sIL-1RA) and intracel-

Received May 26, 2004; revision received November 5, 2004; accepted November 10, 2004.

From the Divisions of Cardiology (H.L., H.H., T.Y., R.E., M.H., R.W., K.T., K.Y., H.C., Y.O., K.K., M.K., Y.A.) and Clinical Nephrology and Rheumatology (H.M.), Niigata University Graduate School of Medical and Dental Sciences, and Department of Medical Technology, School of Health Sciences, Faculty of Medicine (M.N.), Niigata University, Niigata, and Division of Stem Cell Regulation Research, Osaka University Medical School (J.M.), Suita, Japan.

Correspondence to H. Hanawa, Division of Cardiology, Niigata University Graduate School of Medical and Dental Sciences, 1-757 Asahimachi-dori, Niigata 951-8120, Japan. E-mail hanawa@med.niigata-u.ac.jp

Circulation **is available at http://www.circulationaha.org** **DOI: 10.1161/01.CIR.0000160348.75918.CA**

lular IL-1RA (icIL-1RA).[12] IL-1RA functions as an antagonist by competitively binding to IL-1RI.[13,14] IL-1RA cannot transduce intracellular signals because it is unable to bind to IL-1Racp.[12,15] IL-1RA–based therapies are being evaluated for a variety of diseases.[16–18]

The purpose of the present study was to investigate whether IL-1RA transduction ameliorated EAM and by what mechanisms this therapy occurred. Hydrodynamics-based gene transfer via the rapid tail vein injection of a large volume is more efficient than delivery by intramuscular injection with electroporation.[19,20] This method can retrogradely deliver plasmid DNA predominantly into hepatocytes via hepatic vein. Moreover, chimeras with immunoglobulin (Ig) facilitate elevated concentration levels.[21] In this study, we examined the efficacy of hydrodynamics-based delivery of plasmid DNA encoding an IL-1RA-Ig chimera.

Methods

Animals

Seven-week-old male Lewis rats were purchased from Charles-River Laboratories, Japan (Atsugi, Kanagawa, Japan) and were maintained in our animal facilities. Throughout the studies, all the animals were treated in accordance with the guidelines for animal experiments as laid out by our institute.

Induction of EAM

Cardiac myosin was prepared from the ventricular muscle of porcine hearts as previously described.[1] To produce EAM, each rat was immunized on day 0 with 0.2 mL emulsion containing cardiac myosin with an equal volume of complete Freund's adjuvant by a single subcutaneous injection in both footpads.

In Vivo Treatment of EAM With Plasmid DNA Encoding IL-1RA-Ig Gene

Construction of Plasmid DNA for Gene Transfer

We first constructed the plasmid vector pCAGGS-Ig-glucagon (Glu)-tag, containing *Swa*I and *Not*I restriction sites, via polymerase chain reaction (PCR) amplification. For this purpose, initial PCR products were generated from rat spleen cDNA using KOD Plus DNA polymerase (Toyobo) and the following primers: 5′-gaGAATTCATTTAAATgagaGCGGCCGCgtgcccagaaactgtg-3′ (contains both *Swa*I and *Not*I restriction sites) and 5′-tcaaccactgcacaaaatcttgggctttacccggagagtgggagagact-3′. The final PCR product inserts were then amplified from the diluted products of the first PCR reaction with the following primers: 5′-gaGAATTCATTTAAATgagaGCGGCCGCgtgcccagaaactgtg-3′ (as before) and 5′-gagagagaGAATTCtcaggtattcatcaaccac-tgcacaaaattcttgggc-3′. Finalized PCR products were inserted into the pCAGGS vector using *Eco*RI sites. *Escherichia coli* JM109 competent cells were then transformed, and recombinant plasmids were isolated by use of a Quantum Prep Plasmid Maxiprep kit (Bio-Rad Laboratories). To construct the control plasmid, pCAGGS-rat signal peptide (SP)-Ig-Glu-tag, the SP region of secretory leukocyte protease inhibitor, was amplified from EAM heart cDNA with the primers 5′-gaGAATTCATTTAAATgaagtccagcggcctcttcccc-3′ and 5′-gcagcatcGCGGCCGCtccttccacactccagggtgccag-3′, followed by insertion into pCAGGS-Ig-Glu-tag using *Swa*I and *Not*I sites. To construct the pCAGGS-mouse IL-1RA-Ig-Glu-tag, mouse IL-1RA was amplified from mouse splenocyte cDNA using the primers 5′-gagaattcATTTAAATggaaatctgctggggaccctac-3′ and 5′-gcagcatc GCGGCCGCttggtcttcctggaagtagaact-3′, followed by insertion into pCAGGS-Ig-Glu-tag using *Swa*I and *Not*I sites. Recombinant plasmids were isolated as described above.

Plasmid DNA Injection Techniques

Nineteen rats were divided into 2 groups, the pCAGGS-IL-1RA-Ig group (IL-1RA-Ig group; n=10) and the pCAGGS-SP-Ig group (SP-Ig group; n=9). Rats were injected with 800 μg pCAGGS-mouse IL-1RA-Ig-Glu-tag or pCAGGS-SP-Ig-Glu-tag via the tail vein within 15 seconds (receiving ≈80 mL/kg body weight) on day 1.[19]

Plasmid Chimeric Glucagons-Tag Protein Measurement

Blood samples were taken on days 2, 5, 8, 12, and 17. Glucagon concentrations were measured with a glucagons radioimmunoassay kit (Daiichi Radioisotope Laboratories).[22] Chimeric protein concentrations in blood were calculated with Glu-tag.[23] To observe the relationship of them and gene expression in liver, the livers were harvested on days 2, 5, 8, 12, and 17 after injection of pCAGGS-IL-1RA-Ig-Glu-tag into normal rats (n=4, respectively), and transgene expressions were examined by real-time reverse-transcriptase (RT) PCR using the following primers: 5′-tctgactgaccgcgttactccca-3′ (726 to 748 bases in pCAGGS) and 5′-atcagtgatgttaacttcctccag-3′ (316 to 339 bases in mouse sIL-1RA).

Evaluation of Echocardiography and Hemodynamic Parameters

On day 17, echocardiography was performed with a 7.5-MHz probe (SSD-630, Aloka ECHO camera). Left ventricular (LV) internal diameter in end diastole and end systole, interventricular septal thickness, LV posterior wall thickness, pericardial effusion (PE) under LV posterior wall thickness, and LV fractional shortening were calculated from M-mode echocardiograms over 3 consecutive cardiac cycles.

The hemodynamic parameters were measured after echocardiography. Mean arterial pressure was recorded through a catheter introduced into the right femoral artery. Central venous pressure (was recorded through a catheter introduced into the confluence of the vena cava with the right jugular vein. A catheter-tip transducer was inserted into the left ventricle from the right carotid artery to measure the peak left ventricular pressure and left ventricular end-diastolic pressure. The rates of intraventricular pressure rise and decline (±dP/dt) were measured with a differential amplifier. Heart rate was calculated from ECGs. All hemodynamic parameters were recorded on a thermostylus recorder after a stabilizing period of 10 minutes.

Evaluation of Histopathology

Heart and body weights were measured, and the ratio of heart weight to body weight (g/g) was calculated. Several transverse sections were cut from the midventricle slice and stained with Azan-Mallory. The myocarditis area of each specimen was determined with a color image analyzer (Mac SCOPE version 2.6, Mitani Corp).

Measurement of Atrial Natriuretic Peptide mRNA Levels

To measure mRNA levels of atrial natriuretic peptide (ANP), a heart failure marker, total RNA was isolated from the apical one third of the heart on day 17. The absolute copy number of ANP mRNA was measured by quantitative real-time RT-PCR.

Gene Expression of IL-1 Family in EAM Hearts

To evaluate crosstalk between members of the IL-1 family, the mRNA levels of IL-1α, IL-1β, IL-1RI, IL-1RII, IL-1Racp, sIL-1RA, or total IL-1RA (sIL-1RA+icIL-1RA) in both isolated and purified cells from EAM hearts were measured. On day 18, cardiomyocytes and the other cells in the hearts of EAM rats were isolated after collagenase perfusion treatment for 20 minutes with a Langendorff apparatus as reported previously.[24,25] Isolated cells, while maintained in an isotonic buffer, were separated serially through stainless steel sieves into cardiomyocytes and the other cells. Because the inflammatory cells are almost $CD11b^+$ cells (macrophages/dendritic cells/granulocytes) and $\alpha\beta$T cells,[3] the other cells without cardiomyocytes were separated into $\alpha\beta$T cells, $CD11b^+$ cells, and noncardiomyocytic noninflammatory (NCNI) cells (mainly fibroblasts, smooth

TABLE 1. Absolute Copy Numbers of Specific Cell Marker mRNA in Cultivated Cells

	Copy Numbers of mRNA/μg of Total RNA	
	NC Cells (n=6)	Lymph Node Cells (n=6)
CD3	37 600±6300	1 490 000±215 000
Collagen type III	149 000 000±10 500 000	170 000±15 000
Calponin	23 400 000±2 110 000	ND
CD11b	11 800 000±977 000	19 000±4200
von Willebrand factor	194 000±31 000	262 000±56 000
α-Cardiac myosin	ND	ND

Results are expressed as mean±SEM.

muscle cells, and endothelial cells) by anti-PE micro beads (Miltenyi Biotec) and an MACS magnetic cell sorting system (Miltenyi Biotech) using appropriate monoclonal antibodies, namely PE-conjugated TCRα/β (R73) and CD11bc (OX-42) (Pharmingen).[26] The fractions of cardiomyocytes, αβT cells, $CD11b^+$ cells, and NCNI cells were confirmed by analysis of specific marker gene expression—α-cardiac myosin, CD3, CD11b, collagen type III, calponin, and von Willebrand factor—and even if the level of contamination was the highest, it was <10% (data not shown). Total RNA was isolated from each purified cell fraction (cardiomyocytes, n=5; αβT cells, n=5; $CD11b^+$ cells, n=5; NCNI cells, n=6). The absolute copy numbers of IL-1 family mRNA were measured by quantitative real-time RT-PCR.

Cell Culture With Serum Containing IL-1RA-Ig

NC Cells

On day 18, NC cells were isolated from the hearts of EAM rats via collagenase preparation and were cultured for 1 week on 35-mm–well dishes in 3 mL RPMI medium supplemented with 10% FCS. These cultivated NC cells were suggested to contain mainly fibroblasts, smooth muscle cells, and $CD11b^+$ cells, as determined by gene expression analysis (Table 1). After reaching confluence, NC cells were stimulated by addition of 10 ng/mL IL-1α (Pepro Tech) and 100 μL IL-1RA-Ig-Glu-tag–containing serum (30 nmol/L) or the same amount of Ig-Glu tag–containing serum (IL-1RA-Ig+IL-1α group, n=6; SP-Ig+IL-1α group, n=6; no serum and no IL-1α group, n=6). After culture for 24 hours at 37°C, NC cells were collected and total RNA was isolated. The absolute copy numbers of γ-actin, prostaglandin E synthase (PGES), cyclooxygenase-2 (Cox-2), and IL-1β mRNA were measured by quantitative real-time RT-PCR.

Lymphocytes

Lymphocytes isolated from popliteal lymph nodes of EAM rat were prepared in 3 mL RPMI medium supplemented with 10% FCS in 35-mm–well dishes. These cells were thought to be mainly lymphocytes, as indicated by expression of the CD3 gene (Table 1). Because transfer of concanavalin A (Con-A)–stimulated lymphocytes from EAM popliteal lymph nodes could induce EAM[27] and Con-A–stimulated lymphocytes can express the IL-1RI gene (data not shown), we stimulated these cells with 10 μg/mL Con-A (Sigma) and 10 ng/mL IL-1α at 6×10^6 cells per dish. One hundred microliters of IL-1RA-Ig-Glu-tag–containing serum (30 nmol/L) or the same amount of Ig-Glu-tag–containing serum was added (IL-1RA-Ig+Con-A+IL-1α, n=6; SP-Ig+Con-A+IL-1α, n=6; no serum, no Con-A, and no IL-1α, n=6). After culture for 24 hours at 37°C, these cells were collected and total RNA was isolated. The absolute copy numbers of γ-actin, IL-2, and IFN-γ mRNA were measured by quantitative real-time RT-PCR.

Quantitative Real-Time RT-PCR Analysis

Total RNA was extracted by use of Trizol (Invitrogen). cDNA was synthesized from 2 to 5 μg total RNA with random primers and murine Moloney leukemia virus RT. To create the plasmids used for the standard, the cDNAs for ANP, specific cell markers, IL-1 family proteins, and immunologic molecules were amplified from an EAM heart–derived cDNA library with the primers indicated in Table 2. PCR-amplified cDNA inserts were directly inserted into the pGEM-T easy vector, and the recombinant plasmids were isolated, after transformation into *E coli* JM109 competent cells, with the MagExtractor plasmid kit (Toyobo). Diluted plasmid and cDNA were amplified via real-time RT-PCR with a Lightcycler, together

TABLE 2. List of Primers for Quantitative RT-PCR

	Sense Primer	Antisense Primer
ANP	5′-atggatttcaagaacctgctagac-3′	5′-gctccaatcctgtcaatcctac-3′
α-Cardiac myosin	5′-acaaggttaaaaacctgacagagg-3′	5′-tactgttctgctgactgatgtcaa-3′
CD3	5′-gatcccaaactctgctatatgcta-3′	5′-ctttcatgccaatctcactgtag-3′
CD11b	5′-gggatccgtaaagtagtgagaa-3′	5′-aaaggagctggtacttcctgtct-3′
Collagen type III	5′-cgcaattgcagagacctgaa-3′	5′-acagtcatgggactggcatttat-3′
von Willebrand factor	5′-agaggctacacatctctcagaagc-3′	5′-gaccttcttcttcttgaaaccttg-3′
Calponin	5′-aacataggaaatttcatcaaagcc-3′	5′-gtagactgatagttgcctgatcca-3′
IL-1α	5′-aagttcctgacttgtttgaagacc-3′	5′-gtcatcttcagtaaagggctgatt-3′
IL-1β	5′-gctagtgtgtgatgttcccattag-3′	5′-cttttccatcttcttctttgggta-3′
IL-1RI	5′-ataaactgatggtgatgaatgtgg-3′	5′-tgagagtgaactttcttttggctg-3′
IL-1RII	5′-gttatgacatttacctacgagggc-3′	5′-ctttgtgactggatcaaaaatcag-3′
IL-1Racp	5′-ctggacttaccctgatctggtacg-3′	5′-acacgtgatattgtgaataccctg-3′
sIL-1RA	5′-tctctctccttctcatccttctgt-3′	5′-atcagtgatgttaacctcctccag-3′
Total IL-1RA	5′-agaagaaaagatagacatggtgcc-3′	5′-actttgtgactgtacagggctctt-3′
IL-2	5′-ctgagagggatcgataattacaaga-3′	5′-attggcactcaaatttgttttcag-3′
IFN-γ	5′-atctggaggaactggcaaaaggacg-3′	5′-ccttaggctagattctggtgacagc-3′
PGES	5′-gtgatggagaacagccaggt-3′	5′-gaggaccacgaggaaatgtatc-3′
Cox-2	5′-tgtgatattctcaaacaggagcat-3′	5′-aaggaggatggagttgttgtagag-3′
γ-Actin	5′-agccttccttcctgggcatggagt-3′	5′-tggaggggcctgactcgtcatact-3′

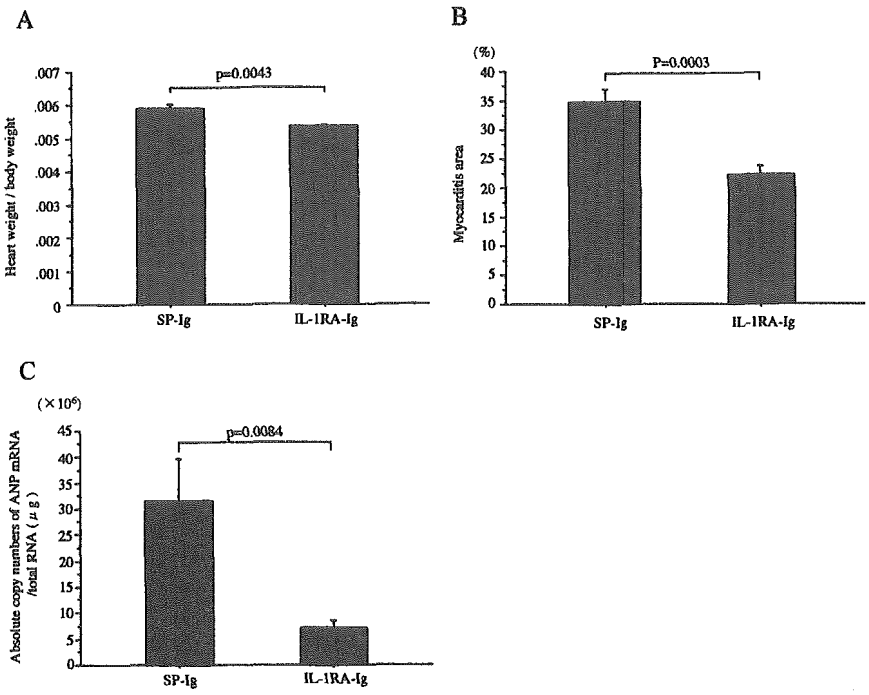

Figure 1. A, Ratio of heart weight to body weight. B, Myocarditis area in EAM heart. Area was calculated by color image analyzer using specimens stained with Azan-Mallory. C, Absolute copy number of ANP mRNA in EAM hearts. Error bars represent SEM. Statistical assessment was performed by unpaired Student *t* test. SP-Ig indicates rats that were injected with pCAGGS-rat SP-Ig-Glu-tag; IL-1RA-Ig, rats injected with pCAGGS-mouse IL-1RA-Ig-Glu-tag.

with the same primer pair used for making the plasmid and a LightCycler-FastStart DNA Master SYBR Green I kit (Roche). After an initial denaturation step of 10 minutes at 95°C, a 3-step cycling procedure (denaturation at 95°C for 10 seconds, annealing at 62°C for 10 seconds, and extension at 72°C for 13 seconds) was used for 40 cycles. The absolute copy numbers of particular transcripts were calculated by LightCycler software using a standard curve approach.[4] cDNA from cultivated cells was then subjected to quantitative RT-PCR analysis, with the level of γ-actin mRNA acting as an internal control.

Statistical Analysis

Statistical assessment was performed by unpaired Student *t* test or 1-way ANOVA and Bonferroni multiple comparison test. The differences were considered significant at $P<0.05$. Ratio of heart weight to body weight, myocarditis area, echocardiography and hemodynamic parameters, data obtained from quantitative RT-PCR, and concentration of IL-1RA-Ig-Glu-tag and Ig-Glu-tag were expressed as mean±SEM.

Results

Effect of In Vivo Treatment With Plasmid DNA Encoding IL-1RA-Ig Gene

The heart to body weight ratios in the IL-1RA-Ig group were significantly lower than those of the SP-Ig group (mean±SEM, 0.53±0.03% versus 0.59±0.05%; $P=0.0043$) (Figure 1A). The inflammatory area in the IL-1RA-Ig group was significantly smaller than that observed in the SP-Ig group (22.3±4.8% versus 34.6±6.8%, $P=0.0003$) (Figure 1B). Expression of ANP mRNA (a heart failure marker) was significantly lower in heart tissues of the IL-1RA-Ig group than those of controls ($7.13\times10^6\pm3.62\times10^6$ versus $31.6\times10^6\pm24.2\times10^6$ copy/total RNA μg; $P=0.0084$) (Figure 1C).

Echocardiograph and Hemodynamic Parameters

As shown in Table 3, the LV fractional shortening and the absolute value of +dP/dt or −dP/dt in IL-1RA-Ig group were significantly larger than in SP-Ig group. LV end-systolic diameter, LV posterior wall thickness, PE, LV end-diastolic pressure, and central venous pressure were significantly smaller in the IL-1RA-Ig group than in SP-Ig group.

Time Course of IL-1RA-Ig-Glu-Tag Protein Levels

Plasma IL-1RA-Ig-Glu-tag protein levels in the IL-1RA-Ig group were found to increase, peaking at 23.21±8.52 nmol/L (mean±SEM) on day 2, and gradually decrease to 5.56±2.70 nmol/L on day 5, 1.64±0.63 nmol/L on day 8, 0.85±0.45 nmol/L on day 12, and 0.22±0.07 nmol/L on day 17. The plasma Ig-Glu-tag protein levels in the SP-Ig group were seen

TABLE 3. Echocardiographic and Hemodynamic Parameters

	IL-1RA-Ig (n=7)	SP-Ig (n=6)	*P*
LVEDd, mm	5.41±0.05	5.48±0.29	0.81
LVESd, mm	3.01±0.17	3.81±0.24	0.018
IVS, mm	1.84±0.05	1.96±0.12	0.33
LVPW, mm	1.89±0.17	2.24±0.27	0.012
PE, mm	1.71±0.47	3.67±0.49	0.016
LVFS, %	44.4±2.9	30.4±2.4	0.0039
HR, bpm	354.9±14.3	381.5±19.8	0.29
CVP, mm Hg	1.73±0.26	3.93±0.55	0.0029
AP, mm Hg	78.4±2.52	72.6±1.72	0.094
LVP, mm Hg	91.1±3.53	85.9±2.08	0.244
EDP, mm Hg	11.7±1.3	18.4±2.24	0.0218
+dP/dt, mm Hg/s	4459±243	3636±178	0.0226
−dP/dt, mm Hg/s	−5547±352	−4129±202	0.0067

LVEDd indicates LV end-diastolic internal diameter; LVESd, LV end-systolic internal diameter; IVS, interventricular septal thickness; LVPW, LV posterior wall thickness; LVFS, LV fractional shortening; HR, heart rate; CVP, central venous pressure; AP, mean blood pressure; LVP, peak LV pressure; EDP, LV end-diastolic pressure; +dP/dt, maximum dP/dt; and −dP/dt, minimum dP/dt.

Result are expressed as mean±SEM.

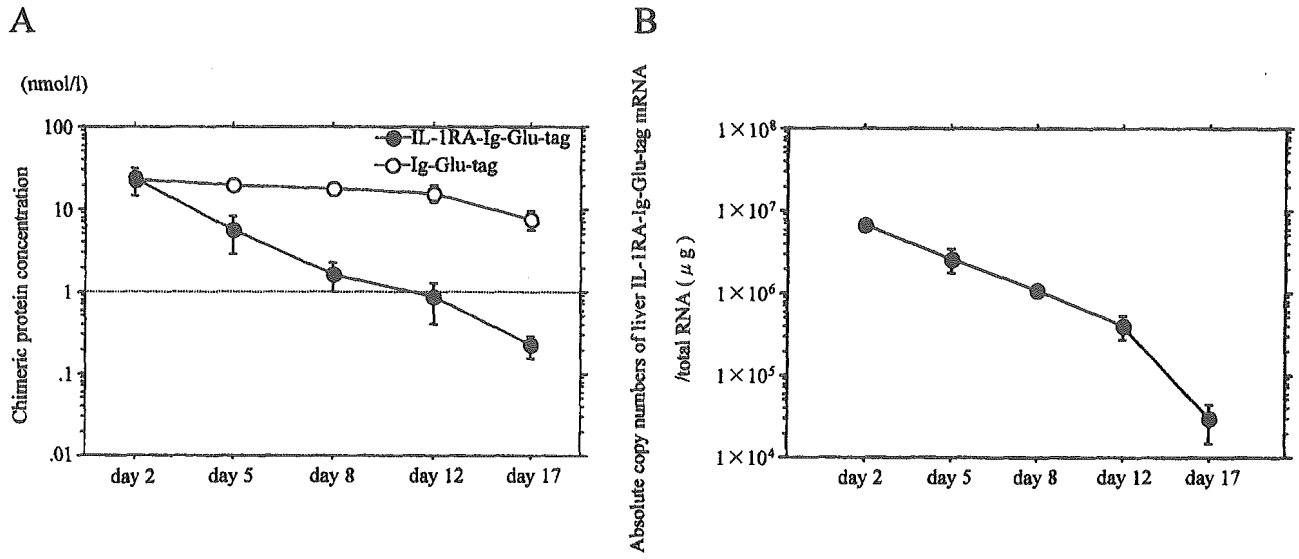

Figure 2. A, Plasma IL-1RA-Glu-tag protein and Ig-Glu-tag protein levels. Chimeric protein concentrations were calculated by use of Glu-tag. B, Absolute copy numbers of IL-1RA mRNA in liver (n=4). Error bars represent SEM. IL-1RA-Ig-Glu-tag indicates rats injected with pCAGGS-mouse IL-1RA-Ig-Glu-tag; Ig-Glu-tag, rats injected with pCAGGS-rat SP-Ig-Glu-tag.

to increase, peaking at 22.75±2.34 nmol/L on day 2, and gradually decrease to 19.48±1.62 nmol/L on day 5, 17.50±2.50 nmol/L on day 8, 15.59±3.56 nmol/L on day 12, and 7.45±1.88 nmol/L on day 17 (Figure 2A). The expressions of IL-1RA-Ig-Glu-tag transferred into normal rat liver by hydrodynamics-based gene delivery were similar to plasma IL-1RA-Ig-Glu-tag protein levels (Figure 2B). It has been reported that IL-1RA (1 to 10 ng/mL, 0.05 to 0.5 nmol/L) suppresses the production of PGES from rat astrocytes stimulated by lipopolysaccharide in vitro.[28] These results indicated that continuous effective delivery of IL-1RA-Ig protein for >16 days can be achieved in rats by hydrodynamics-based transfection.

Gene Expression of IL-1 Family in Purified Cells From EAM Hearts

Both IL-1α and IL-1β were strongly expressed in CD11b$^+$ cells. The IL-1RI gene was strongly expressed in NCNI cells (the cell fraction containing mainly fibroblasts, smooth muscle cells, and endothelial cells) and $\alpha\beta$T cells, whereas the IL-1RII gene was found to be markedly expressed in CD11b$^+$ cells. The IL-1Racp gene was strongly expressed in both CD11b$^+$ and NCNI cells and was moderately expressed in $\alpha\beta$T cells. Both total IL-1RA and sIL-1RA were detected in CD11b$^+$ cells. These results suggested that IL-1, produced mainly by CD11b$^+$ cells, acted on NCNI and $\alpha\beta$T cells by binding to IL-1RI and transduced intracellular signals by forming with IL-1Racp. On the other hand, CD11b$^+$ cells also produced native IL-1RA and IL-1RII, potentially suppressing the action of IL-1 (Figure 3).

Expression of Immunologic Molecules in Cultivated Cells With Serum Containing IL-1RA-Ig

IL-1RA-Ig–containing serum significantly reduced expression of PGES (mean±SEM, 1.22±0.22 versus 1.94±0.17; P<0.0001), Cox-2 (0.93±0.24 versus 2.00±1.05; P=0.0092), and IL-1β (3.91±1.22 versus 11.25±2.16; P<0.0001) at the mRNA level in cultivated NC cells (the cell fraction containing mainly fibroblasts, smooth muscle cells, and CD11b$^+$ cells) (Figure 4). In addition, IL-1RA-Ig–containing serum significantly reduced expression of the IL-2 (0.0004±0.0001 versus 0.0310±0.0090; P<0.0001) and IFN-γ (0.0065±0.0036 versus 0.0461±0.0385; P=0.0091) genes in cultivated lymphocytes (Figure 5).

Discussion

In the present study, we demonstrated that hydrodynamics-based delivery of plasmid DNA encoding the IL-1RA-Ig gene ameliorated EAM. IL-1RA-Ig–affecting cells were thought to be NCNI cells (fibroblasts, smooth muscle cells, and endothelial cells) and $\alpha\beta$T cells because IL-1RI and IL-1Racp were found in them. Endogenous IL-1α and IL-1β produced mainly by CD11b$^+$ cells, especially secreted IL-1β, influence these surrounding cells in a paracrine manner. IL-1RA-Ig, generated after gene transfer, appears to inhibit the IL-1–induced reactions of these cells and ameliorates EAM.

The functions of IL-1 with respect to cell regulation are varied.[29] In this study, the effect of serum containing IL-1RA-Ig on the mRNA expression of various immunologic molecules in cultivated NC cells (mainly fibroblasts, smooth muscle cells, and CD11b$^+$ cells) from hearts and lymphocytes from popliteal lymph nodes of EAM rats was investigated. The concentration of IL-1RA-Ig in cultivated cells was almost the same as that observed at the onset of myocarditis (day 10 to 11) and that reported by previous in vitro studies to be an effective dose.[28,30] In this study, there was a 30- to 50-fold increase in the expression of PGES, Cox-2, and IL-1β mRNA in NC cells by IL-1 alone, but the increase was significantly reduced by serum containing IL-1RA-Ig. PGE2 produced by PGES plays an important role in inflammation and pain.[31] In rheumatoid arthritis, the level of PGES detected

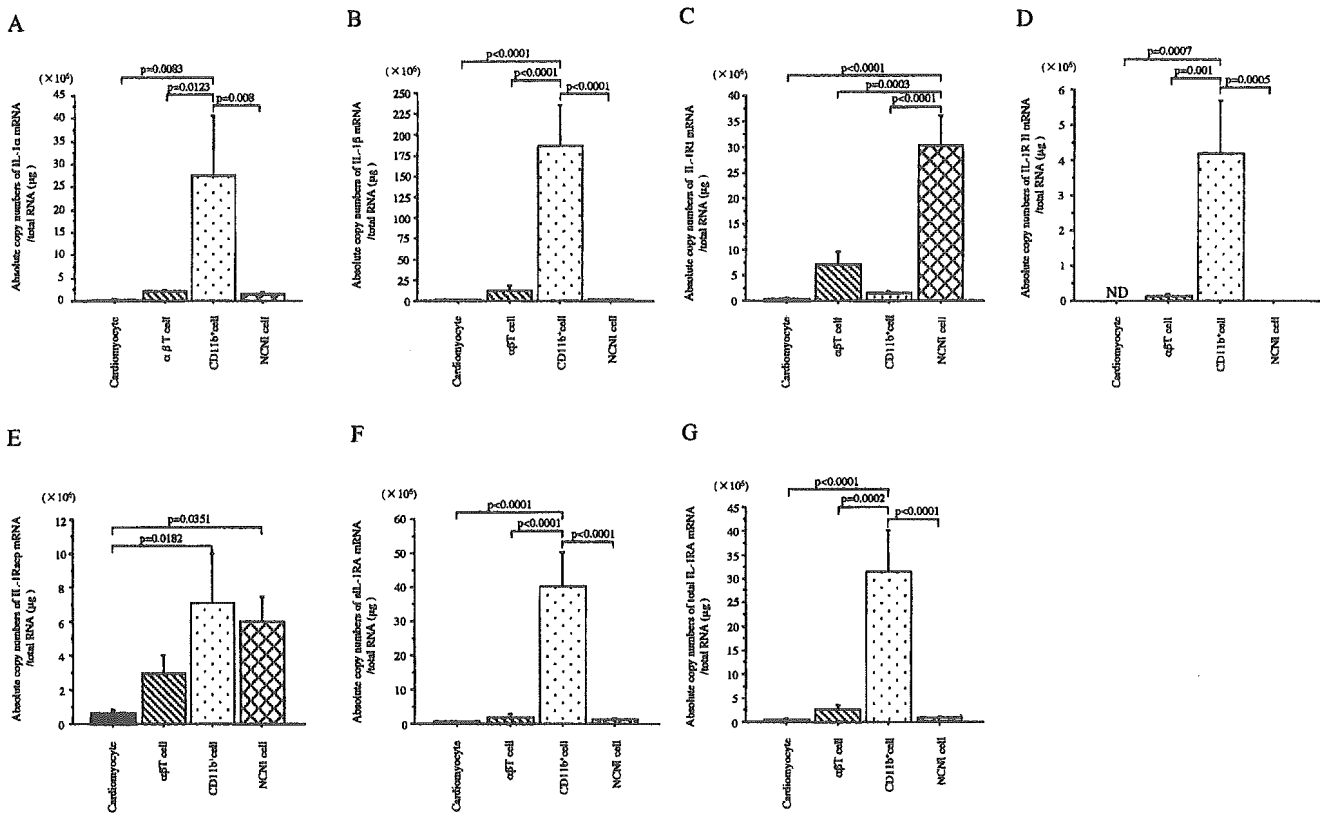

Figure 3. A through G, Absolute copy numbers of IL-1α, IL-1β, IL-1RI, IL-1RII, IL-1Racp, sIL-1RA, and total IL-1RA, respectively. Each cell was separated and purified from EAM heart on day 18. Error bars represent SEM. Statistical assessment was performed by 1-way ANOVA and Bonferroni multiple comparison test. Differences were considered significant at $P<0.05$.

at the inflammatory region is very high.[32] Our study of PGES and Cox-2 gene expression in purified cells from EAM hearts indicated that they were produced mainly by NCNI cells and slightly by $CD11b^+$ cells (data not shown). IL-1RA-Ig may inhibit the expression of the PGES and Cox-2 gene directly on NCNI cells via IL-1R. IL-1–induced IL-1 production has been shown in various cell types.[33] IL-1RA-Ig may also inhibit IL-1 production directly on NCNI cells. However, because our study indicated that IL-1 was produced mainly by $CD11b^+$ cells, IL-1RA-Ig may inhibit IL-1 production of $CD11b^+$ cells indirectly via NCNI cells or $\alpha\beta$T cells. Reduced PGES, Cox-2, and/or IL-1 production by NC cells in EAM hearts may be an effect resulting in improved myocarditis. On the other hand, in lymphocytes of popliteal lymph node, IL-2 and IFN-γ mRNA expression levels were significantly reduced by serum containing IL-1RA-Ig. In EAM,

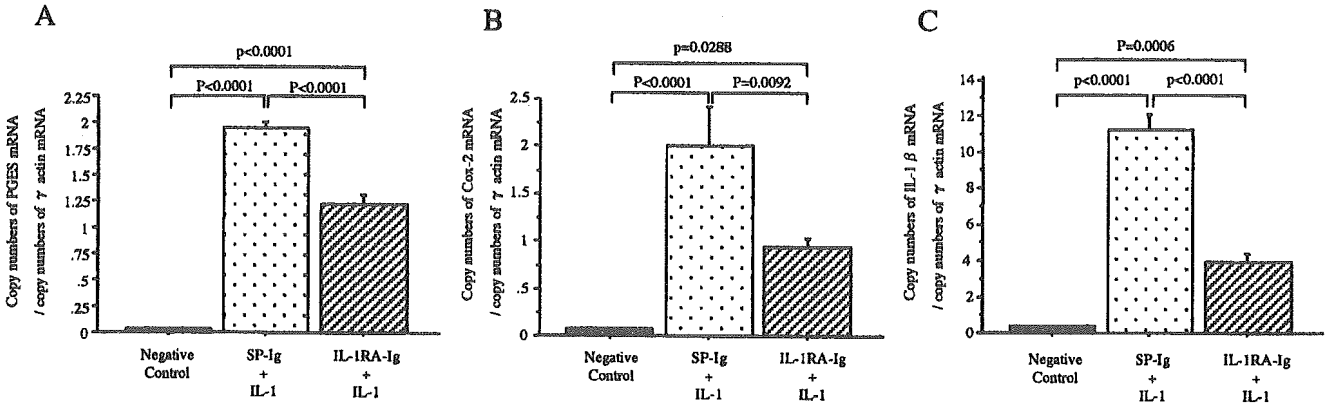

Figure 4. Copy numbers of various immunologic molecules mRNA/copy numbers of γ-actin mRNA in NC cells cultivated from EAM hearts. A, PGES; B, Cox-2; C, IL-1β. Negative control cells were cultivated in medium without IL-1α and rat serum. SP-Ig+IL-1 cells were cultivated in medium with IL-1α and rat serum treated with pCAGGS-SP-Ig-Glu-tag; IL-1RA-Ig+IL-1 cells were cultivated in medium with IL-1α and rat serum treated with pCAGGS-mouse IL-1RA-Ig-Glu-tag. Error bars represent SEM. Statistical assessment was performed by 1-way ANOVA and Bonferroni multiple comparison test. Differences were considered significant at $P<0.05$.

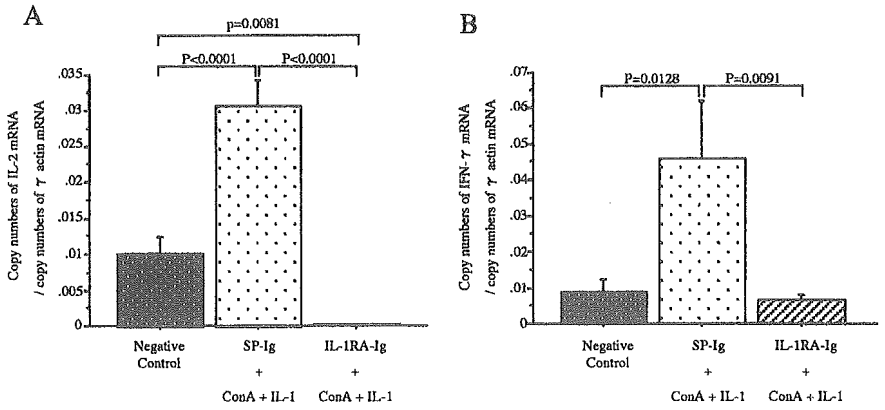

Figure 5. Copy numbers of various immunologic molecules mRNA/copy numbers of γ-actin mRNA in cultivated lymphocytes from swollen lymph node of EAM. A, IL-2; B, IFN-γ. Negative control cells were cultivated in medium without Con-A, IL-1α, and serum. SP-Ig+Con-A+IL-1 cells were cultivated in medium with Con-A, IL-1α, and rat serum treated with pCAGGS-SP-Ig-Glu-tag. IL-1RA-Ig+Con-A+IL-1 cells were cultivated in medium with Con-A, IL-1α, and rat serum treated with pCAGGS-mouse IL-1RA-Ig-Glu-tag. Error bars represent SEM. Statistical assessment was performed by 1-way ANOVA and Bonferroni multiple comparison test. Differences were considered significant at $P<0.05$.

which is a T cell–mediated disease,[27] Th1 cytokines such as IL-2 and IFN-γ produced by $CD4^+$ T cells are thought to play a central role.[4] Therefore, inhibition of Th1 cytokine production by IL-1RA-Ig may improve EAM.

In human rheumatoid arthritis, it has been reported that Anakinra (a recombinant form of IL-1RA) suppressed progression of this disease,[34] and treatment with IL-1RA has been investigated in various animal models.[16–18] Therefore, the number of diseases in which IL-1RA has a therapeutic relevance may be extended in the near future. Human myocarditis is serious and often fatal despite intensive care. However, the cause of myocarditis is not usually evident. It was reported that gene therapy with IL-1RA expression plasmid was effective in the treatment of viral myocarditis and reduced virus titer in hearts.[18] Here, we demonstrated that IL-1RA-Ig gene transfer ameliorated EAM resembling human giant cell myocarditis. Therefore, treatment with IL-1RA may be effective for acute and fulminant myocarditis even if its cause is unknown.

Hydrodynamics-based gene delivery of plasmid DNA as used in this study is both inexpensive and highly effective in terms of facilitating gene expression. The concentration of IL-1RA-Ig in blood obtained by this method was higher compared with plasmid DNA transfection into muscle with in vivo electroporation.[19,20] The producing cells to which plasmid DNA is transferred by this method are thought to be mainly hepatocytes. Plasmid DNA is thought to be delivered into hepatocytes by retrograde blood flow from hepatic veins. If plasmid DNA encoding IL-1RA-Ig can be directly transfected into the heart, T cells and NCNI cells in EAM hearts will be highly influenced by IL-1RA-Ig, and EAM may be ameliorated. Hou et al[35] reported heart-targeted plasmid DNA transfer by retrograde coronary vein using a balloon catheter. This method, which is easy and not very risky, may be suitable for human clinical application. New developments of this gene therapy can be expected in the future.

References

1. Kodama M, Matsumoto Y, Fujiwara M, Masani F, Izumi T, Shibata A. A novel experimental model of giant cell myocarditis induced in rats by immunization with cardiac myosin fraction. *Clin Immunol Immunopathol.* 1990;57:250–262.
2. Kodama M, Hanawa H, Saeki M, Hosono H, Inomata T, Suzuki K, Shibata A. Rat dilated cardiomyopathy after autoimmune giant cell myocarditis. *Circ Res.* 1994;75:278–284.
3. Kodama M, Zhang S, Hanawa H, Shibata A. Immunohistochemical characterization of infiltrating mononuclear cells in the rat heart with experimental autoimmune giant cell myocarditis. *Clin Exp Immunol.* 1992;90:330–335.
4. Hanawa H, Abe S, Hayashi M, Yoshida T, Yoshida K, Shiono T, Fuse K, Ito M, Tachikawa H, Kashimura T, Okura Y, Kato K, Kodama M, Maruyama S, Yamamoto T, Aizawa Y. Time course of gene expression in rat experimental autoimmune myocarditis. *Clin Sci (Lond).* 2002;103:623–632.
5. March CJ, Mosley B, Larsen A, Cerretti DP, Braedt G, Price V, Gillis S, Henney CS, Kronheim SR, Grabstein K. Cloning, sequence and expression of two distinct human interleukin-1 complementary DNAs. *Nature.* 1985;315:641–647.
6. Scala G, Allavena P, Djeu JY, Kasahara T, Ortaldo JR, Herberman RB, Oppenheim JJ. Human large granular lymphocytes are potent producers of interleukin-1. *Nature.* 1984;309:56–59.
7. Rupp EA, Cameron PM, Ranawat CS, Schmidt JA, Bayne EK. Specific bioactivities of monocyte-derived interleukin 1 alpha and interleukin 1 beta are similar to each other on cultured murine thymocytes and on cultured human connective tissue cells. *J Clin Invest.* 1986;78:836–839.
8. Baldari C, Murray JA, Ghiara P, Cesareni G, Galeotti CL. A novel leader peptide which allows efficient secretion of a fragment of human interleukin-1 beta in Saccharomyces cerevisiae. *EMBO J.* 1987;6:229–234.
9. Sims JE, Acres RB, Grubin CE, McMahan CJ, Wignall JM, March CJ, Dower SK. Cloning the interleukin 1 receptor from human T cells. *Proc Natl Acad Sci U S A.* 1989;86:8946–8950.
10. Wesche H, Korherr C, Kracht M, Falk W, Resch K, Martin MU. The interleukin-1 receptor accessory protein (IL-1RAcP) is essential for IL-1–induced activation of interleukin-1 receptor–associated kinase (IRAK) and stress-activated protein kinases (SAP kinases). *J Biol Chem.* 1997;272:7727–7731.
11. Colotta F, Re F, Muzio M, Bertini R, Polentarutti N, Sironi M, Giri JG, Dower SK, Sims JE, Mantovani A. Interleukin-1 type II receptor: a decoy target for IL-1 that is regulated by IL-4. *Science.* 1993;261:472–475.
12. Arend WP, Malyak M, Guthridge CJ, Gabay C. Interleukin-1 receptor antagonist: role in biology. *Annu Rev Immunol.* 1998;16:27–55.
13. McIntyre KW, Stepan GJ, Kolinsky KD, Benjamin WR, Plocinski JM, Kaffka KL, Campen CA, Chizzonite RA, Kilian PL. Inhibition of interleukin-1 (IL-1) binding and bioactivity in vitro and modulation of acute inflammation in vivo by IL-1 receptor antagonist and anti-IL-1 receptor monoclonal antibody. *J Exp Med.* 1991;173:931–939.
14. Dinarello CA. The interleukin-1 family: 10 years of discovery. *FASEB J.* 1994;8:1314–1325.
15. Guo C, Dower SK, Holowka D, Baird B. Fluorescence resonance energy transfer reveals interleukin (IL)-1–dependent aggregation of IL-1 type I receptors that correlates with receptor activation. *J Biol Chem.* 1995;270:27562–27568.
16. Badovinac V, Mostarica-Stojkovic M, Dinarello CA, Stosic-Grujicic S. Interleukin-1 receptor antagonist suppresses experimental autoimmune encephalomyelitis (EAE) in rats by influencing the activation and proliferation of encephalitogenic cells. *J Neuroimmunol.* 1998;85:87–95.
17. Kim JM, Jeong JG, Ho SH, Hahn W, Park EJ, Kim S, Yu SS, Lee YW, Kim S. Protection against collagen-induced arthritis by intramuscular gene therapy with an expression plasmid for the interleukin-1 receptor antagonist. *Gene Ther.* 2003;10:1543–1550.

18. Nakano A, Matsumori A, Kawamoto S, Tahara H, Yamato E, Sasayama S, Miyazaki JI. Cytokine gene therapy for myocarditis by in vivo electroporation. *Hum Gene Ther.* 2001;12:1289–1297.
19. Maruyama H, Higuchi N, Nishikawa Y, Kameda S, Iino N, Kazama JJ, Takahashi N, Sugawa M, Hanawa H, Tada N, Miyazaki J, Gejyo F. High-level expression of naked DNA delivered to rat liver via tail vein injection. *J Gene Med.* 2002;4:333–341.
20. Liu F, Song YK, Liu D. Hydrodynamics-based transfection in animals by systemic administration of plasmid DNA. *Gene Therapy.* 1999;6: 1258–1266.
21. Jiang J, Yamato E, Miyazaki J. Sustained expression of Fc-fusion cytokine following in vivo electroporation and mouse strain differences in expression levels. *J Biochem (Tokyo).* 2003;133:423–427.
22. Nishino T, Kodaira T, Shin S, Imagawa K, Shima K, Kumahara Y, Yanaihara C, Yanaihara N. Glucagon radioimmunoassay with use of antiserum to glucagon C-terminal fragment. *Clin Chem.* 1981;27: 1690–1697.
23. Hanawa H, Watanabe R, Hayashi M, Yoshida T, Abe S, Komura S, Liu H, Elnaggar R, Chang H, Okura Y, Kato K, Kodama M, Maruyama H, Miyazaki J, Aizawa Y. A novel method to assay proteins in blood plasma after intravenous injection of plasmid DNA. *Tohoku J Exp Med.* 2004; 202:155–161.
24. Hwang TC, Horie M, Nairn AC, Gadsby DC. Role of GTP-binding proteins in the regulation of mammalian cardiac chloride conductance. *J Gen Physiol.* 1992;99:465–489.
25. Isenberg G, Klockner U. Calcium tolerant ventricular myocytes prepared by preincubation in a "KB medium." *Pflugers Arch.* 1982;395:6–18.
26. Toba K, Hanawa H, Fuse I, Sakaue M, Watanabe K, Uesugi Y, Higuchi W, Takahashi M, Aizawa Y. Difference in CD22 molecules in human B cells and basophils. *Exp Hematol.* 2002;30:205–211.
27. Kodama M, Matsumoto Y, Fujiwara M. In vivo lymphocyte-mediated myocardial injuries demonstrated by adoptive transfer of experimental autoimmune myocarditis. *Circulation.* 1992;85:1918–1926.
28. Pistritto G, Ciabattoni G, Mancuso C, Tringali G, Preziosi P, Navarra P. Signaling pathways involved in lipopolysaccharide stimulation of prostaglandin production by rat hypothalamic astroglial cells. *J Endotoxin Res.* 2000;6:307–311.
29. Dinarello CA. Interleukin-1 and interleukin-1 antagonism. *Blood.* 1991; 77:1627–1652.
30. Rambaldi A, Torcia M, Dinarello CA, Barbui T, Cozzolino F. Modulation of cell proliferation and cytokine production in AML by recombinant interleukin-1 receptor antagonist. *Leukemia.* 1993;7:S10–S12.
31. Trebino CE, Stock JL, Gibbons CP, Naiman BM, Wachtmann TS, Umland JP, Pandher K, Lapointe JM, Saha S, Roach ML, Carter D, Thomas NA, Durtschi BA, McNeish JD, Hambor JE, Jakobsson PJ, Carty TJ, Perez JR, Audoly LP. Impaired inflammatory and pain responses in mice lacking an inducible prostaglandin E synthase. *Proc Natl Acad Sci U S A.* 2003;100:9044–9049.
32. Stichtenoth DO, Thoren S, Bian H, Peters-Golden M, Jakobsson PJ, Crofford LJ. Microsomal prostaglandin E synthase is regulated by proinflammatory cytokines and glucocorticoids in primary rheumatoid synovial cells. *J Immunol.* 2001;167:469–474.
33. Warner SJ, Auger KR, Libby P. Human interleukin 1 induces interleukin 1 gene expression in human vascular smooth muscle cells. *J Exp Med.* 1987;165:1316–1331.
34. Fleischmann RM. Addressing the safety of anakinra in patients with rheumatoid arthritis. *Rheumatology (Oxford).* 2003;42:ii29–ii35.
35. Hou D, Maclaughlin F, Thiesse M, Panchal VR, Bekkers BC, Wilson EA, Rogers PI, Coleman MC, March KL. Widespread regional myocardial transfection by plasmid encoding Del-1 following retrograde coronary venous delivery. *Catheter Cardiovasc Interv.* 2003;58:207–211.